
ON THE TRANSITION FROM NEURAL REPRESENTATION TO SYMBOLIC KNOWLEDGE

Junyan Cheng
Thayer School of Engineering
Dartmouth College
Hanover, NH 03755
jc.th@dartmouth.edu

Peter Chin
Thayer School of Engineering
Dartmouth College
Hanover, NH 03755
pc@dartmouth.edu

August 7, 2023

ABSTRACT

Bridging the huge disparity between neural and symbolic representation can potentially enable the incorporation of symbolic thinking into neural networks from essence. Motivated by how human gradually builds complex symbolic representation from the prototype symbols that are learned through perception and environmental interactions. We propose a Neural-Symbolic **Transitional Dictionary Learning (TDL)** framework that employs an EM algorithm to learn a transitional representation of data that compresses high-dimension information of visual parts of an input into a set of tensors as neural variables and discover the implicit predicate structure in a self-supervised way. We implement the framework with a diffusion model by regarding the decomposition of input as a cooperative game, then learn predicates by prototype clustering. We additionally use RL enabled by the Markovian of diffusion models to further tune the learned prototypes by incorporating subjective factors. Extensive experiments on 3 abstract compositional visual objects datasets that require the model to segment parts without any visual features like texture, color, or shadows apart from shape and 3 neural/symbolic downstream tasks demonstrate the learned representation enables interpretable decomposition of visual input and smooth adaption to downstream tasks which are not available by existing methods.

1 Introduction

Symbols, such as languages, mathematics, and signs, are crucial in human thinking and represent key aspects of System II intelligence Chandler [2022], Kahneman [2011]. However, modern Neural Networks (NN) often lack essential capabilities like interpretability, compositionality, and logical reasoning, which are inherent in symbolic thinking. As a result, there is growing interest in imbuing NN with System II intelligence.

Existing approaches overlook a crucial fact: the neural representations learned by current NN, focused on data compression, are not well-suited for System II tasks that require explicit structural information, such as properties and relations. For instance, while humans perceive a character as strokes organized by structures, typical machine learning algorithms view it as a combination of principal components. This difference in representation hinders the adoption of symbolic thinking in NN.

To bridge this gap between neural and symbolic representations, we propose a Transitional Dictionary Learning (TDL) framework. It leverages the Expectation-Maximization (EM) algorithm to learn a transitional representation that combines the advantages of both neural and symbolic representations. This representation compresses high-dimensional information into tensors as neural variables and learns predicate structures within and between those variables. The learned representation allows the model to decompose input images into interpretable visual parts and embeds implicit relations. Examples are presented in Figure 1.

To implement the framework, we model the decomposition process as a cooperative game of parts solved by a diffusion model. We use prototype clustering on the decomposed parts to learn implicit predicates. To obtain parts aligned

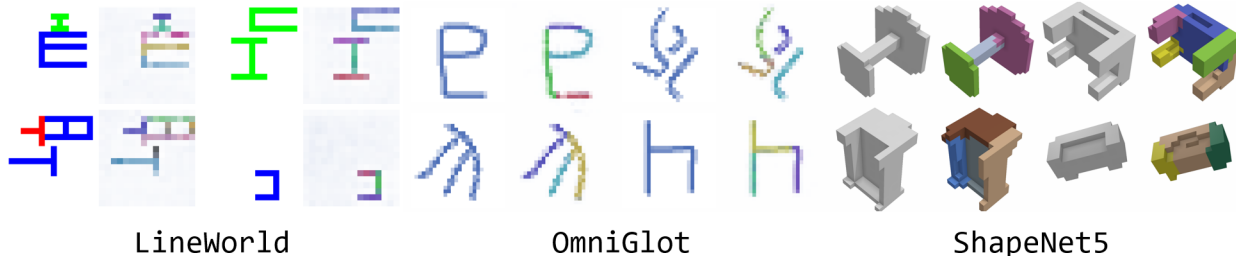


Figure 1: Interpret samples from three datasets as visual parts marked with different colors, shallowness represents confidence. The left in each pair is input, the right is interpretation.

with human intuition, we experiment with Reinforcement Learning (RL) to incorporate subjective human factors and preferences that evolved through complex symbol emergence processes.

To evaluate whether the model really learned a dictionary of meaningful concepts and relations or only a visual pattern recognizer, we experiment with our method on a novel task of decomposing abstract compositional visual objects, as shown in Figure 1, there are no visual features including edges, color difference, or texture in the objects shown in our datasets, which are the basis for vision models to distinguish different objects and parts, thus the only way to separate the strokes out is the concept of strokes, therefore, decomposing the abstract objects in our datasets into meaningful parts gives a strong indicator that the model discovers symbolic concepts and relations. To the best of our knowledge, there is no existing method that can achieve this.

We conduct experiments on three datasets comprising abstract compositional visual objects and evaluate them across three downstream tasks involving symbol grounding and transfer learning. The results demonstrate that our method effectively learns the transitional representation, allowing interpretable decomposition of data and seamless adaptation to neural and symbolic tasks. We are the first method to learn to segment abstract objects into parts without relying on visual features like texture, edges, shadows, or color differences. Our supplementary materials include code and datasets, publicly available for further exploration.

2 Dictionary Learning for Transitional Representation

We formulate the transitional representation in Section 2.1, we learn such a transitional representation by optimizing the features of both neural and symbolic representations simultaneously under a dictionary learning framework, the neural part illustrated in Section 2.2, and the symbolic part discussed in Section 2.3, we combine them to get our TDL framework, finally, we derive a metric for evaluating the learned dictionary in Section 2.3.3.

2.1 Transitional Representation

An ideal transitional representation should provide structural information like properties and relations of the compositions of the input while not losing the compression ability of high-dimension data. The structural information can be represented as *predicates*, which are broadly applied in symbolic AI that are hypothesized to be able to represent all intelligent activities Newell and Simon [1976], and isomorphic to typical symbolic systems from Curry-Howard correspondence Howard [1980] and its extensions. Our transitional representation learns implicit predicates in different arys and orders in multiple dictionaries.

We assume that an input x can be represented as a set of atomic sentences $\Omega = \{\rho_1^1(\cdot), \rho_2^1(\cdot), \dots, \rho_1^2(\cdot, \cdot), \rho_2^2(\cdot, \cdot), \dots\}$ of predicates from different order and arity. For a 1-ary sentence $\rho^1(r)$: when ρ^1 is first-order, r is a logical variable tensor represented by NN; when ρ is higher-order, r is the neural representation for another sentence. Similar for N-ary cases. The model learns to predict logic variables R which compressed high-dimension information of input x by $P(R|x, D)$ that embeds potential sentences $P(\Omega|R, D, x)$, that can depict the input in a meaningful way, based on D , the learned dictionaries of different ary/order predicates.

We use a deep learning model to implicitly learn the dictionary that allows it to use multiple vectors as neural variables to compress an input while learning to let the output vectors be implicitly organized by discovered predicates. There are infinity ways of choosing the variables, the challenge comes in three folds, firstly, the variables should accurately compress the information from the original input, secondly, the variables are expected to be meaningful and

interpretable, for example, we wish for compressed strokes instead of principle components to be the variables when given a handwritten character, thirdly, the found variables should be the ones that can form meaningful relations each other, for example, we expect the strokes are the ones that can be reused for composing different characters.

2.2 Learning Neural Features

The first challenge discussed above of compressing high-dimension information corresponds to the neural features of the learned representation. We formulate it in the dictionary learning framework. Given the dataset $X = \{x_1, \dots, x_n\}$, we learn a dictionary $D = \{d_1, \dots, d_n\}$, $D \in \mathbb{R}^{d \times n}$, to explain the data. we assume an input x_i is composed by $f(\vec{r}_i; D)$ where $\vec{r}_i = (r_i^1, \dots, r_i^m)$ and $r_i^j \in \mathbb{R}^d$ is the set of neural variables, each variable is transformed from a prototype $d_k \in D$ in the dictionary by $r_i^j = T(d_k)$, f is a composition function describes how x_i is composed of \vec{r}_i .

The target of a sparse dictionary learning Kreutz-Delgado et al. [2003] is

$$\arg \min_{D, r_i} \sum_i \epsilon(x_i, f(\vec{r}_i; D)) + \lambda |\vec{r}_i|, |d_i| < 1, \forall d_i \in D \quad (1)$$

it learns to give parsimony explanations with sparse representations and compress the high-dimension information by minimizing the reconstruction error ϵ . Specifically, the original sparse dictionary learning applies the reconstruction function $f(\vec{r}_i; D) = D\vec{r}_i$ and error $\epsilon(x_i, f(\vec{r}_i; D)) = \|x_i - f(\vec{r}_i; D)\|_2^2$ which assumes the data generation process to be linear and the reconstruction in pixel space. In Formula 1, we relax these assumptions to enable more complex compositional processes, such as the composition of parts instead of the linear combination of vector components. The representation that meets the first challenge that can be learned by optimizing this formula.

2.3 Learning Symbolic Features

To tackle the remaining two challenges we discussed at the end of Section 2.1, we need to learn to let the variables \vec{r}_i embed predicate structure. To simplify the problem, we restrict the variables of an image to be the parts of it. However, there are still infinitely many ways to segment an image as parts while we expect only the ‘‘meaningful’’ ones. The criteria of ‘‘meaningful’’ can be varied, including both objective and human subjective ones.

We regard the objective ones can be learned without supervision, while the subjective ones should be learned by aligning with humans. We assume that the objective criteria already allow a good initial segmentation, which can be tuned to a subjective good one with low-cost tunings. We’ll focus on self-supervised learning towards the objective criteria in this section, and later we will discuss how to align human preference later.

2.3.1 Reduce to Subword tokenization

Finding objective criteria that allow us to segment an input image into meaningful parts is non-trivial. One criterion actually implied in the third challenge is that the parts should be easily reusable to form compositions with each other. By regarding the reusable parts as prototypes in the dictionary. Our task is to find the most common reusable composable prototypes from a set of images to build the dictionary.

This is identical to the subword tokenization problem which tries to build the dictionary by finding frequently used subwords in a corpus of sentences. Subword means the split points inside a sentence can be arbitrary instead of only space or commas. Subword tokenizer learns to segment the sequence of characters from sentences into subwords based on a learned dictionary. While in images, the model learns to segment parts from the pixels matrix using the learned dictionary. By analogy pixels as characters, parts as words, images as sentences, dataset as corpus, and ignoring the difference in structures (i.e. sequence vs matrix) and dictionary (i.e. discrete vs continuous) for now, we may reduce our problem to subword tokenization, and then put the simplified parts back.

Subword tokenization can be formulated as decomposing a given sentence string s into a sequence of subwords $\vec{s} = (s^1, \dots, s^n)$ using a dictionary D where $s^i \in D$. Kudo and Richardson [2018] introduces ULM that solves this problem with the EM algorithm, it initializes a huge dictionary randomly or heuristically, then iterate E and M steps to remove terms from the dictionary until the dictionary reaches an ideal size.

In the E-step, sentences are decomposed by the Viterbi algorithm with the current dictionary $D^{(t)}$ as $\vec{s}_i^t = \arg \max_{\vec{s}_i \in U(s_i)} P(\vec{s}_i^t)$, where $P(\vec{s}_i^t) = \prod_{j=1}^m P(s_i^j)$ assumes a 1-gram Harris [1954] language model, $U(s_i)$ is the set of all possible decomposition of s_i , the likelihood of corpus is $L(D^{(t)}) = \sum_{i=1}^N P(\vec{s}_i^t)$. In the M-step, measure the contribution of each dictionary term by $l(d) = L(D^{(t)}) - L(D^{(t)} - \{d\})$ as the likelihood loss if remove a term d , then maximize the expectation by removing the terms with lowest contribution (e.g. 20%) from $D^{(t)}$ to get $D^{(t+1)}$.

2.3.2 Neural-Symbolic Transitional Dictionary Learning

The ULM learns an efficient dictionary of terms that can be frequently reused, we will extend this EM algorithm back to our problem for learning a dictionary of reusable prototypes. To put it in our problem, we firstly generalize sentence inputs to our visual input $x_i = f(\vec{r}_i; D)$, where \vec{r}_i are neural variables that correspond to visual parts, then generalize the Viterbi algorithm to a decomposition function $\vec{r}_i = g(x_i; \theta, D)$ parameterized by θ and dictionary D to sample the candidate segmentations of image.

The reusability of words in ULM relies on the 1-gram language model. Extend to images, the likelihood of a dataset can be computed as $\log P(X) = \sum_{i=1}^n \log \sum_{j=1}^{m_i} \log P(r_i^j)$, where m_i is the length of \vec{r}_i follows $r_i^j = T(d_q)$ where $d_q \in D$. Maximizing it is essentially clustering the r_i^j with d_q as centroids, it implicitly discovers the property or category information of the parts, i.e. the *1-ary predicate*.

However, the 1-gram assumption may omit rich relations between parts. A natural extension is the N-gram, where the likelihood of an input x_i is $\log P(r_i) = \sum_{j=1}^{m_i} \log P(r_i^j | r_i^{1:j})$, for example, a 2-gram model is $\log P(r_i) = \sum_{j=1}^{m_i} \log P(r_i^j | r_i^{j-1})$. However, the Markov assumption for N-gram does not fit for non-sequential structures such as images, thus we use a joint probability $P(r_i^p, r_i^q, \dots, r_i^k)$ over an arbitrary subset of the decomposed terms instead.

It implicitly models the association among the N terms, which gives relational information and thus learns an *N-ary predicate*, for example, when $N = 2$, it models the highly-correlated pairs (r_i^p, r_i^q) that may exhibit some relationship. The higher-order predicates model more complex relations, like the association over associations, e.g. $P((r_i^k, r_i^j; \rho_1), (r_i^p, r_i^q; \rho_2))$, the association between two pairs associated with predicates ρ_1 and ρ_2 respectively. We can learn predicates of different order and arity by using different probabilistic assumptions.

Based on this idea, a flexible EM framework for learning predicates of any order and any-ary through different probabilistic assumptions of $P(\vec{r}_i)$ can be given:

$$E - Step : Q(\theta | \theta^{(t)}) = E_{D \sim P(\cdot | R, \theta^{(t)})} [\log P(R, D | \theta)] \quad (2)$$

$$M - Step : \theta^{(t+1)} = \arg \min_{\theta^{(t+1)}} Q(\theta^{(t+1)} | \theta^{(t)}) \quad (3)$$

where $R = \{r_i^j, i \in [1, n], j \in [1, m_i]\}$ is the set of all terms decomposed from dataset X . By learning multiple dictionaries of different ary and order of predicates over the decomposed parts R , the decomposed parts will tend to be the ones that can be frequently reused in different relations and categories over the dataset which meets the remaining challenges we discussed in Section 2.1. Thus introduce the “*symbolic*” features to the representation.

By optimizing this EM framework in Formulas 2, 3, along with the sparse dictionary learning in Formula 1 at the same time, the learned representation should embed both neural and symbolic features. We propose it as our **Transitional Dictionary Learning (TDL)** framework. We will introduce our implementation of the TDL framework in Section 3.

2.3.3 Clustering Information Gain

Given the learned representation, a problem is how to evaluate whether it meets our objective criteria of learning reusable compositions. We may evaluate it by viewing whether the parts shown in the decompositions can be clustered to a few centroids which means the parts applied are highly reusable.

Based on this idea, we propose the Clustering Information Gain (CIG) by comparing the Mean Clustering Error (MCE) of the decomposed terms in the test set, marked as $MCE = [\sum_{i=1}^n \sum_{j=1}^{m_i} (\min_{d \in D} \|r_i^j - d\|_2) / m_i] / n \propto -L(\theta)$ with the random decomposition, MCE_{rand} , which is a lower-bound when the decomposed terms are randomly scattered, while the best case of MCE is 0 when the compositions perfectly explained by learned concepts. CIG is defined as $1 - \frac{MCE_{model}}{MCE_{rand}}$ gives a score normalized in $[0, 1]$ therefore giving us an intuitive indicator. More details in Appendix D.4.

3 Method

To implement the TDL framework, we need to first implement a segmentation network that gives an image as input, it can output a set of masks where each mask corresponds to a part for the Formula 2, we compose the parts and compare it with the input for the Formula 1, then a clustering of the decomposed parts from the training set in the Formula 3. We use a diffusion model that solves the cooperative game of parts as the segmentation network in Section 3.1, then we introduce prototype clustering in Section 3.2. Figure 2 shows an overview of our architecture. Furthermore, we propose RL to tune the representation with subjective criteria in Section 3.3.

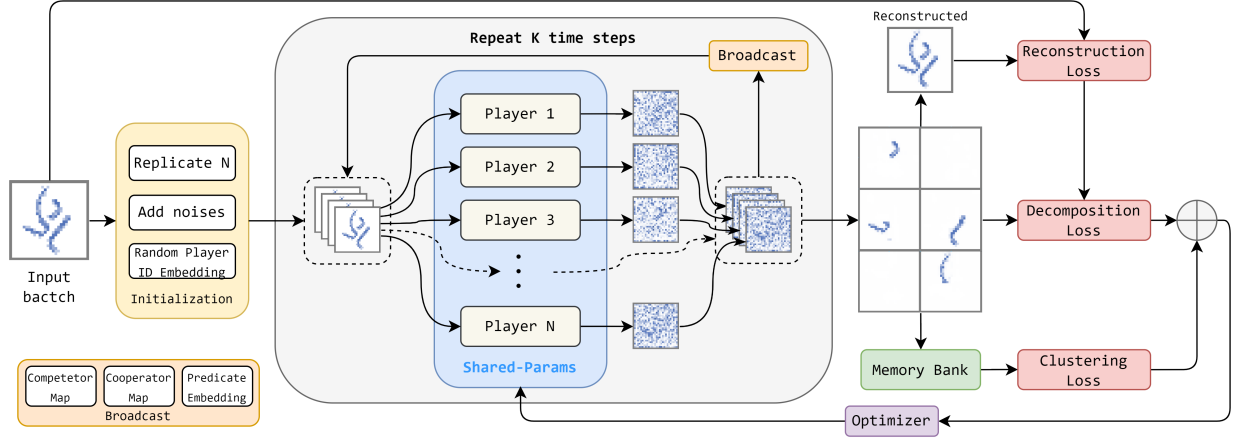


Figure 2: Overview our architecture. The diffusion model decomposes a training image into visual parts for computing decomposition loss including the reconstruction loss, then be clustered with memory banks of different dictionaries for computing clustering error.

3.1 Game-Theory inspired Decomposition

Precise unsupervised pixel-wise masks of the input can be obtained from attention map Dosovitskiy et al. [2020], Hamilton et al. [2022], or clustering pixel-wise features Amir et al. [2021] with Transformers, or generated by diffusion models Wu et al. [2022] with U-Nets. In our tasks, the dataset sizes are relatively small which is not effective to train a Transformer-based model, while Wu et al. [2022] shows how diffusion models generate accurate masks on small datasets, we also apply a diffusion model to implement the segmentation network.

We formulate the segmentation network as the encoder and decoder parts. Given a visual input $x_i \in R^{H \times W \times C}$, we assume 2D input here which can be easily extended to 3D voxels, the encoder network $\vec{r} = g(x; \theta, D)$ generate a set of neural variables \vec{r} that can be decoded as parts of image $x_i^j = f_g(r_i^j)$ by f_g , the input can be simply reconstructed through $x_i = \sum_{j=1}^{m_j} x_i^j$. The encoder can be viewed as the downsampling part in UNet while the decoder is the upsampling part.

3.1.1 Decomposition as cooperative game

The challenge is that different inputs may have different numbers of parts which demands a self-organized way to dynamically preserve only meaningful parts. Inspired by Gemp et al. [2021] which models PCA as a competitive game where players are candidate principle components moved by changing its value, we also model the decomposition process as the cooperative game of the parts.

We randomly initialized N_P neural variables \vec{r} as players move by adjusting the values, where N_P is a hyper-parameter, the players cooperatively reconstruct the input, while competing by avoiding repeating each other, and the ones whose corresponding part $x^j = f_g(r^j)$ is empty are dropped. The utilities of the game are modeled by a GT loss

$$L_{GT} = L_{Reconstruction} + \alpha_1 L_{Overlap} + \alpha_2 L_{resources} + \alpha_3 L_{norm} \quad (4)$$

It evaluates the equilibrium state reached by N_P players with image parts $\vec{x} = (x^1, x^2, \dots, x^{N_P})$. $L_{Overlap}$ avoids the player repeating each other as competition, $L_{resources}$ avoids the extreme case where one player does the entire job while others are empty, L_{norm} regularizes the action space, and **Reconstruction loss** $L_{Reconstruction}$ is the cooperative target. We leave more details about the loss function design in Appendix B.2.

3.1.2 Game Playing as Markov Process

Players move in the direction that maximizes the utility $-L_{GT}$, the optimal move for a player j given by gradient $\nabla_{r_i^j} L_{GT}$ which is expansive to compute. Instead, we train an actor network $r_i^j(t+1) = Actor(s_i^j(t); \theta_A, D)$ to output the move for player j based on current state $s_i^j(t)$ and dictionaries $D \in R^{N_D \times dim_D}$. The state encodes useful information for taking action about competitors, cooperators, and input.

The game proceeds with K steps, in each step, players take action and then broadcast their moves to update the state of each other, this results in a Markov process $P(r_i^j(t+1)|s_i^j(t); D)$ for each player j , we implement it as a score-based diffusion model SMLD Song et al. [2021].

The move of a player can be sampled by the Langevin dynamics $r_i^j(t+1) = r_i^j(t) + \epsilon \nabla_{r_i^j(t)} L_{GT} + \sqrt{2\epsilon} z(t), z(t) \sim N(0, I), t = 0, 1, \dots, K$ where ϵ is the step size, the gradient approximated by a scoring function, implemented as our actor-network, that minimizes $E_x[\|\nabla_r L_{GT}(x) - Actor(s; \theta_A, D)\|^2]$ which is trained by a target L_{SMLD} from SMLD. We apply this loss as a regularization which results in the **Decomposition loss** $L_{Decomposition} = L_{GT} + \beta L_{SMLD}$. The decomposition of the input obtained in the equilibrium of the game. In our experiments, a few steps are enough to converge, thus we do full samplings for each sample during training. More details about our diffusion model architectural design and optimizations can be found in Appendix B.1.

3.2 Prototype Clustering of Predicates

We initialize terms as prototype vectors for each dictionary, then iteratively optimize them by K-Means clustering. Clustering all neural variables R for the entire dataset every time is expensive and the distribution is shifting as the segmentation network update. Thus, we maintain a FIFO memory bank $M = (m_0, \dots, m_L)$ of size L for each dictionary, for 1-ary predicates, $m = f_m^1(r^i)$ maps a neural logic variable r^i to a representation $m \in \mathbb{R}^{dim_m}$, for 2-ary, $m = f_m^2(r^i, r^j)$ maps a pair (r^i, r^j) , and similar for higher order and arity. Specifically, a pair representation computed as $m_{(i,j)} = f_m^2(f_g(r^i) + f_g(r^j))$ in our work then mapping with convolution layers. By storing the most recent decomposed parts, M can be assumed to be generated from a steady distribution.

The clustering executes every one or a few training steps, starting after warming up epochs. Similar to Caron et al. [2018], we run K-Means on set $\vec{m} + M$ for each dictionary, where $\vec{m} = (m_1^1, m_1^2, \dots, m_2^1, m_2^2, \dots, m_B^{N_P})$ is the set of mapped logic variables in a batch of length B , we drop unwanted terms like empty ones and randomly sample pairs to improve efficiency.

The clustering gives assignments C for each term in \vec{m} , we create pseudo labels Y for terms in \vec{m} by assigning prototypes in dictionary D for their nearest clustering centroids given by C . Then try to move the prototype closer to the centroid and the samples closer to the prototype in latent space by minimizing the Cross-Entropy (CE) loss $\min_{D, \theta} CE_{Loss}(dist(\vec{m}, D), Y)$, where $dist$ is a distance metric (e.g. L2 distance), compute the current assignment of each term.

The **clustering loss** is defined as the summation of CE loss of all dictionaries $L_{Clustering} = \gamma \sum_{D_i \in D} CE_{Loss}(dist_i, E_i)$. We optimize it with decomposition loss as $L_{TDL} = L_{Clustering} + L_{Decomposition}$ to implement the TDL framework. Detail about the architecture can be found in Appendix B.1.2.

3.3 Tuning by Reinforcement Learning

Benefiting from the Markovian of the game-playing process, we naturally apply Proximal Policy Optimization (PPO) Schulman et al. [2017] to our model. PPO iteratively samples several sequences of the game by the actor-network and then uses these samples to optimize the policy. We train a critic model in addition to predicting the value of a given state $v_i^j(t) = Critic(s_i^j(t); \theta_C, D)$ for PPO. We design a heuristic reward function to encourage “energy-saving” shapes with three criteria, smoothness, solidity, and continuity. See Appendix D.5 for details. We also do an experiment on RL from human feedback in Appendix D.2.

4 Experiment and Analysis

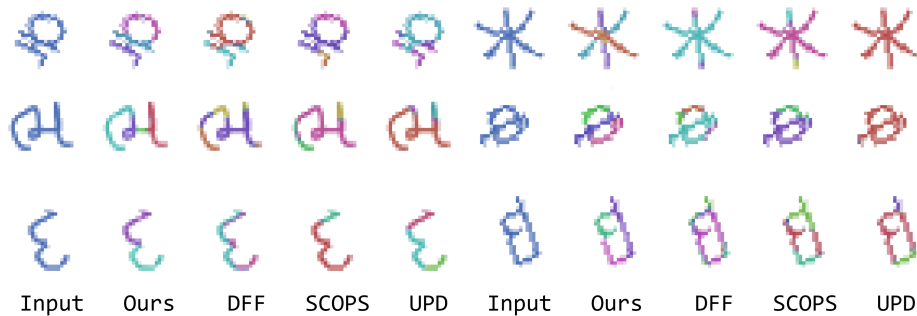


Figure 3: Comparison between our method and baselines on the OmniGlot test set. Our method can learn interpretable strokes compared to the baselines that failed to give effective strokes.

We perform experiments to evaluate whether the TDL framework can learn the representation that embeds both neural and symbolic features. And also explores how we can utilize the representation for the downstream neural and symbolic tasks. We introduce the experiment settings in Section 4.1, and the results are discussed in Section 4.2, we further do downstream tasks in 4.3, and we also do extensive additional experiments in Appendix D to comprehensively analyze the proposed methods.

4.1 Experiment setting

We choose 3 datasets of *abstract* composable visual objects: **LineWorld** is synthesized by the babyARC engine Wu et al. [2022], it uses *lines* as the basic concept and *parallel* and *perpendicular* as basic relations to randomly draw non-overlapping shapes of “F”, “E”, “T”, etc., in each image. **OmniGlot** Lake et al. [2015] consists of handwritten characters with recorded strokes. Each character is implicitly composed hierarchically as subparts and parts from strokes Lake et al. [2015]. **ShapeNet5** consists of 3D shapes in 5 categories (bed, chair, table, sofa, lamp) with shared basic elements Achlioptas et al. [2019] from the ShapeNet database Chang et al. [2015]. We voxelized it by binvox Nooruddin and Turk [2003], Min [2004 - 2019], we replace 2D conv layers with 3D in all methods for this dataset. We further derive 3 downstream tasks based on them, which we will discuss later.

We compare our method with 3 state-of-the-art unsupervised part segmentation methods which are the most similar to our work with completely different motivations, DFF Collins et al. [2018], SCOPS Hung et al. [2019], and UPD Choudhury et al. [2021], which decomposes images into parts as a heatmap of k channels, each channel represents a part. Full details about our baselines, datasets, and splits of the train, dev, test set, hardware settings, and our hyper-param searches can be found in Appendix C.

	LineWorld			OmniGlot			ShapeNet5			LW-G	OG-G	
	IoU	CIG	SP	MAE	CIG	SP	IoU	CIG	SP	IoU	Acc.	IoU
AE	97.7	-	-	0.9	-	-	85.1	-	-	-	-	-
DFF	-	33.1	38.3	-	36.9	33.3	-	20.1	19.2	43.1	28.8	42.8
SCO.	-	35.7	42.4	-	38.6	38.9	-	23.1	24.3	46.8	26.4	46.9
UPD	-	36.3	42.8	-	42.8	37.4	-	25.4	22.6	46.2	28.7	48.9
Ours	94.3	58.0	82.6	1.8	68.5	77.6	79.8	54.6	60.1	78.4	74.8	75.9
w/o RL	93.7	57.0	71.9	2.0	65.1	68.0	78.8	52.9	54.4	78.2	74.3	75.1

Table 1: Results on SSL and symbol grounding, values are multiplied by 100, the higher the better. Ours and w/o RL are our models with and without RL with the heuristic reward model. We compare with a reference Auto-Encoder (AE), and DFF Collins et al. [2018], SCOPS (SCO.) Hung et al. [2019], UPD Choudhury et al. [2021].

4.2 Self-supervised Learning of Transitional representation

Results for SSL of transitional representation are listed in the first three columns in Table 1. We train an Auto-Encoder for each dataset as a reference for the reconstruction error as an indicator of whether high-dimension information is preserved. The inputs LineWorld and ShapeNet5 are binary thus we use IoU for a better intuitive. CIG is proposed in Section 2.3.3. SP is a heuristic Shape score that evaluates whether the parts are natural or not by three continuity, solidity, and smoothness, normalized between 0 and 1.0. The full details of SP are provided in Appendix D.5.

Our model achieves 58.0, 68.5, 54.6 CIG, 82.6, 70.6, and 60.1 SP in the three datasets respectively, significantly better than the baselines which rely on visual features. And the huge advantage keeps even without RL. With a low reconstruction error of 94.3 IoU, 1.8 MAE, and 79.8 IoU compared to the reference. It shows the learned representation can both preserve high-dimension information and learns meaningful parts.

Figure 3 shows a comparison of results between ours and baselines, our method can decompose the inputs into human interpretable strokes, while the baselines do not work for such abstract inputs. We provide extensive additional samples in Appendix G and a qualitative study in Appendix D.6 which shows that our method has much better human interpretability, and the metrics SP and CIG can be good predictors for human interpretability.

4.3 Adapt to downstream tasks

We experiment on two neural and symbolic tasks, symbol grounding and transfer learning. We pre-train our model and baselines then finetune on those tasks.

	Bed			Lamp			Sofa			Table		
	IoU	CIG	SP	IoU	CIG	SP	IoU	CIG	SP	IoU	CIG	SP
w/ PT	67.3	48.1	52.9	61.1	42.1	49.1	62.2	46.8	45.2	68.3	50.1	54.6
w/o PT	18.1	19.0	13.2	18.3	19.9	14.6	21.5	18.9	19.8	19.9	22.1	17.9

Table 2: Transfer learning on ShapeGlot, all values are multiplied by 100, the higher the better.

4.3.1 Symbol grounding

We design two grounding tasks: LW-G is also synthesized with the babyARC engine with given concept masks and relation tuples as labels. The target is to segment the concepts (i.e. lines) and then predict the relations within evaluated by IoU and top-1 accuracy respectively. We align the prediction with ground truth by the minimal overall IoU when evaluating. We pre-train the models on LineWorld. We add a relation prediction head on the top of baselines while our method directly adapts the 2-ary predicate dictionary. OG-G is a subset of OmniGlot with the stroke masks as ground truth, the target is to segment the input as ground truth strokes. We align prediction and ground truth similarly to LW-G, then evaluate by IoU. We pre-train models on OmniGlot without OG-G samples.

Results are reported in Table 1 LW-G and OG-G, we achieved 78.4 IoU, 74.8 Acc. on LW-G and 75.9 IoU on OG-G, largely outperforming baselines whose relation prediction did not converge due to incorrect segmentations. This shows that the learned representation models underlying predicate distribution can be smoother transferred to concrete ones.

4.3.2 Transfer learning

We pre-train on a set of shapes from “chair” and other 4 similar categories, then transfer learning on small sets of 230~550 samples from unseen categories “Bed”, “Lamp”, “Sofa”, “Table” used in ShapeGlot Achlioptas et al. [2019] and compare with the one without pretraining. The results in Table 2 show that the learned representations are reusable and effectively benefit the generalization of neural representation to unseen classes. Without the pre-training, the samples for each class are not even adequate for learning effective decomposition.

5 Related Works

We give a brief review of the related works here. We leave a long related work in Appendix A. **Symbol Emergence.** Studies of primitive symbols in mirror systems Wicker et al. [2003], language evolution theory Petitto [2005], Loockvane [1999] and Broca’s area Arbib [2011], Tomasello [2008], Higuchi et al. [2009] supports a hypothesis proposed that rudimentary symbols emerged in the prehuman brain without human communication Taniguchi et al. [2018]. **Neural-Symbolic AI (NSAI).** specific NSAI applications Segler et al. [2018], Amizadeh et al. [2020], Young et al. [2019], Inala et al. [2020] and general NSAI methods Wang et al. [2019], Cornelio et al. [2023], Dong et al. [2019], Goyal et al. [2021], Vlastelica et al. [2021], Karpas et al. [2022] have been proposed, however, they ignore the NS representation problem. **Compositional Learning.** Compositional knowledge in NN was explored Hinton [2021], Garau et al. [2022], Chen et al. [2020], Mendez and Eaton [2022]. Concept learning composes concepts with primitives Lake et al. [2015], Wu et al. [2022], Mao et al. [2019], Cao et al. [2021], and discover relations Shanahan et al. [2020], Kipf et al. [2020]. We give a general framework to learn predicates without prior compared to current methods. **Unsupervised Segmentation and Parsing.** Unsupervised segmentation Kim et al. [2020], Van Gansbeke et al. [2021], Melas-Kyriazi et al. [2022], and parsing Lin et al. [2020], Bear et al. [2020], Lou et al. [2022], and the co-part segmentation Collins et al. [2018], Hung et al. [2019], Choudhury et al. [2021], Yu et al. [2022], He et al. [2022] were studies. However, they rely on visual features or priors.

6 Discussion

We proposed to learn a transitional representation inspired by the prehuman symbol emergence in this work. However, we do not cover all sides of symbol emergence, such as environmental interactions and social communications Taniguchi et al. [2018], Ma et al. [2022] that has been studied in embodied Gupta et al. [2021] and phylogenetic Ma et al. [2022] intelligence, which implicates a pathway to intelligence by learning from *observation*, *interaction*, then *communication*. For the implementation side, the study on multi-trace diffusion Mariani et al. [2023] may largely improve the performance by accelerating the converging of the game. The game theory design also enables efficient decentralized training Gemp et al. [2021]. Finally, symbolic reasoning may achieve by combining the representation with symbolic modules Mendez and Eaton [2022].

7 Conclusion

In this work, we introduce the TDL framework to learn a transitional representation that embeds both the advantage of neural representations that compress high-dimension information and the symbolic representations that learns concept and relations as predicates. Experiments on SSL and downstream tasks on the abstract visual object datasets show that the learned representation enables meaningful decomposition of objects and smoothly adapts to downstream neural and symbolic tasks which are not available by existing methods that rely on visual features instead of concepts. We believe our work can contribute to the representation learning for NSAI and inspire researchers to discover the mystery of System II intelligence.

References

- P. Achlioptas, J. Fan, R. Hawkins, N. Goodman, and L. J. Guibas. Shapeglot: Learning language for shape differentiation. In *Proceedings of the IEEE/CVF International Conference on Computer Vision*, pages 8938–8947, 2019.
- Amazon. Amazon mechanical turk. <https://www.mturk.com/>, 2005.
- S. Amir, Y. Gandelsman, S. Bagon, and T. Dekel. Deep vit features as dense visual descriptors. *arXiv preprint arXiv:2112.05814*, 2(3):4, 2021.
- S. Amizadeh, H. Palangi, A. Polozov, Y. Huang, and K. Koishida. Neuro-symbolic visual reasoning: Disentangling. In *International Conference on Machine Learning*, pages 279–290. PMLR, 2020.
- M. A. Arbib. The mirror system, imitation, and the evolution of language. *Imitation in animals and artifacts*, 229:38, 2002.
- M. A. Arbib. From mirror neurons to complex imitation in the evolution of language and tool use. *Annual Review of Anthropology*, 40(1):257–273, 2011. doi: 10.1146/annurev-anthro-081309-145722. URL <https://doi.org/10.1146/annurev-anthro-081309-145722>.
- D. Bear, C. Fan, D. Mrowca, Y. Li, S. Alter, A. Nayebi, J. Schwartz, L. F. Fei-Fei, J. Wu, J. Tenenbaum, et al. Learning physical graph representations from visual scenes. *Advances in Neural Information Processing Systems*, 33: 6027–6039, 2020.
- L. Biewald. Experiment tracking with weights and biases, 2020. URL <https://www.wandb.com/>. Software available from wandb.com.
- K. Cao, M. Brbic, and J. Leskovec. Concept learners for few-shot learning. In *International Conference on Learning Representations*, 2021. URL <https://openreview.net/forum?id=eJIJF3-LoZ0>.
- M. Caron, P. Bojanowski, A. Joulin, and M. Douze. Deep clustering for unsupervised learning of visual features. In *Proceedings of the European conference on computer vision (ECCV)*, pages 132–149, 2018.
- M. Caron, I. Misra, J. Mairal, P. Goyal, P. Bojanowski, and A. Joulin. Unsupervised learning of visual features by contrasting cluster assignments. *Advances in neural information processing systems*, 33:9912–9924, 2020.
- D. Chandler. *Semiotics: the basics*. Routledge, 2022.
- A. X. Chang, T. Funkhouser, L. Guibas, P. Hanrahan, Q. Huang, Z. Li, S. Savarese, M. Savva, S. Song, H. Su, et al. Shapenet: An information-rich 3d model repository. *arXiv preprint arXiv:1512.03012*, 2015.
- S. Chen, K. Ma, and Y. Zheng. Med3d: Transfer learning for 3d medical image analysis. *arXiv preprint arXiv:1904.00625*, 2019.
- X. Chen, C. Liang, A. W. Yu, D. Zhou, D. Song, and Q. V. Le. Neural symbolic reader: Scalable integration of distributed and symbolic representations for reading comprehension. In *International Conference on Learning Representations*, 2020. URL <https://openreview.net/forum?id=ryxjnREFwH>.
- J. Cheng, I. Fostiropoulos, and B. Boehm. Gn-transformer: Fusing sequence and graph representation for improved code summarization, 2021a.
- J. Cheng, I. Fostiropoulos, B. Boehm, and M. Soleymani. Multimodal phased transformer for sentiment analysis. In *Proceedings of the 2021 Conference on Empirical Methods in Natural Language Processing*, pages 2447–2458, Online and Punta Cana, Dominican Republic, Nov. 2021b. Association for Computational Linguistics. doi: 10.18653/v1/2021.emnlp-main.189. URL <https://aclanthology.org/2021.emnlp-main.189>.
- S. Choudhury, I. Laina, C. Rupprecht, and A. Vedaldi. Unsupervised part discovery from contrastive reconstruction. In A. Beygelzimer, Y. Dauphin, P. Liang, and J. W. Vaughan, editors, *Advances in Neural Information Processing Systems*, 2021. URL <https://openreview.net/forum?id=iHXQPrISusS>.

- E. Collins, R. Achanta, and S. Susstrunk. Deep feature factorization for concept discovery. In *Proceedings of the European Conference on Computer Vision (ECCV)*, pages 336–352, 2018.
- C. Cornelio, J. Stuehmer, S. X. Hu, and T. Hospedales. Learning where and when to reason in neuro-symbolic inference. In *The Eleventh International Conference on Learning Representations*, 2023. URL <https://openreview.net/forum?id=en9V5F8PR->.
- W.-Z. Dai, Q. Xu, Y. Yu, and Z.-H. Zhou. Bridging machine learning and logical reasoning by abductive learning. *Advances in Neural Information Processing Systems*, 32, 2019.
- J. Devlin, M.-W. Chang, K. Lee, and K. Toutanova. BERT: Pre-training of deep bidirectional transformers for language understanding. In *Proceedings of the 2019 Conference of the North American Chapter of the Association for Computational Linguistics: Human Language Technologies, Volume 1 (Long and Short Papers)*, pages 4171–4186, Minneapolis, Minnesota, June 2019. Association for Computational Linguistics. doi: 10.18653/v1/N19-1423. URL <https://aclanthology.org/N19-1423>.
- G. Di Pellegrino, L. Fadiga, L. Fogassi, V. Gallese, and G. Rizzolatti. Understanding motor events: a neurophysiological study. *Experimental brain research*, 91:176–180, 1992.
- C. Ding, X. He, and H. D. Simon. On the equivalence of nonnegative matrix factorization and spectral clustering. In *Proceedings of the 2005 SIAM international conference on data mining*, pages 606–610. SIAM, 2005.
- H. Dong, J. Mao, T. Lin, C. Wang, L. Li, and D. Zhou. Neural logic machines. In *International Conference on Learning Representations*, 2019. URL <https://openreview.net/forum?id=B1xY-hRctX>.
- A. Dosovitskiy, L. Beyer, A. Kolesnikov, D. Weissenborn, X. Zhai, T. Unterthiner, M. Dehghani, M. Minderer, G. Heigold, S. Gelly, et al. An image is worth 16x16 words: Transformers for image recognition at scale. *arXiv preprint arXiv:2010.11929*, 2020.
- Y. Du, S. Li, and I. Mordatch. Compositional visual generation with energy based models. In H. Larochelle, M. Ranzato, R. Hadsell, M. Balcan, and H. Lin, editors, *Advances in Neural Information Processing Systems*, volume 33, pages 6637–6647. Curran Associates, Inc., 2020. URL https://proceedings.neurips.cc/paper_files/paper/2020/file/49856ed476ad01fcff881d57e161d73f-Paper.pdf.
- Y. Du, S. Li, Y. Sharma, J. Tenenbaum, and I. Mordatch. Unsupervised learning of compositional energy concepts. *Advances in Neural Information Processing Systems*, 34:15608–15620, 2021.
- W. Falcon and The PyTorch Lightning team. PyTorch Lightning, Mar. 2019. URL <https://github.com/Lightning-AI/lightning>.
- V. Gallese, L. Fadiga, L. Fogassi, and G. Rizzolatti. Action recognition in the premotor cortex. *Brain*, 132:1685–1689, 2009.
- Q. Gao, B. Wang, L. Liu, and B. Chen. Unsupervised co-part segmentation through assembly. In *International Conference on Machine Learning*, pages 3576–3586. PMLR, 2021.
- N. Garau, N. Bisagno, Z. Sambugaro, and N. Conci. Interpretable part-whole hierarchies and conceptual-semantic relationships in neural networks. In *Proceedings of the IEEE/CVF Conference on Computer Vision and Pattern Recognition*, pages 13689–13698, 2022.
- A. d. Garcez and L. C. Lamb. Neurosymbolic ai: The 3 rd wave. *Artificial Intelligence Review*, pages 1–20, 2023.
- I. Gemp, B. McWilliams, C. Vernade, and T. Graepel. Eigengame: {PCA} as a nash equilibrium. In *International Conference on Learning Representations*, 2021. URL <https://openreview.net/forum?id=NzTU59SYbNq>.
- Google. Vertex ai data labeling. <https://cloud.google.com/vertex-ai/docs/datasets/data-labeling-job>, 2021.
- A. Goyal, A. Didolkar, N. R. Ke, C. Blundell, P. Beaudoin, N. Heess, M. C. Mozer, and Y. Bengio. Neural production systems. *Advances in Neural Information Processing Systems*, 34:25673–25687, 2021.
- A. Gupta, S. Savarese, S. Ganguli, and L. Fei-Fei. Embodied intelligence via learning and evolution. *Nature communications*, 12(1):5721, 2021.
- M. Hamilton, Z. Zhang, B. Hariharan, N. Snively, and W. T. Freeman. Unsupervised semantic segmentation by distilling feature correspondences. In *International Conference on Learning Representations*, 2022. URL <https://openreview.net/forum?id=SaK06z6H10c>.
- Z. S. Harris. Distributional structure. *Word*, 10(2-3):146–162, 1954.
- X. He, B. Wandt, and H. Rhodin. Ganseg: Learning to segment by unsupervised hierarchical image generation. In *Proceedings of the IEEE/CVF Conference on Computer Vision and Pattern Recognition (CVPR)*, pages 1225–1235, June 2022.

- S. Higuchi, T. Chaminade, H. Imamizu, and M. Kawato. Shared neural correlates for language and tool use in broca’s area. *Neuroreport*, 20:1376–81, 10 2009. doi: 10.1097/WNR.0b013e3283315570.
- G. Hinton. How to represent part-whole hierarchies in a neural network, 2021.
- W. A. Howard. The formulae-as-types notion of construction. In H. Curry, H. B., S. J. Roger, and P. Jonathan, editors, *To H. B. Curry: Essays on Combinatory Logic, Lambda Calculus, and Formalism*. Academic Press, 1980.
- W.-C. Hung, V. Jampani, S. Liu, P. Molchanov, M.-H. Yang, and J. Kautz. Scops: Self-supervised co-part segmentation. In *Proceedings of the IEEE/CVF Conference on Computer Vision and Pattern Recognition*, pages 869–878, 2019.
- J. P. Inala, Y. Yang, J. Paulos, Y. Pu, O. Bastani, V. Kumar, M. Rinard, and A. Solar-Lezama. Neurosymbolic transformers for multi-agent communication. *Advances in Neural Information Processing Systems*, 33:13597–13608, 2020.
- A. Jaiswal, A. R. Babu, M. Z. Zadeh, D. Banerjee, and F. Makedon. A survey on contrastive self-supervised learning. *Technologies*, 9(1):2, 2020.
- C. R. Johnson, E. Hendriks, I. J. Bereznoy, E. Brevdo, S. M. Hughes, I. Daubechies, J. Li, E. Postma, and J. Z. Wang. Image processing for artist identification. *IEEE Signal Processing Magazine*, 25(4):37–48, 2008.
- D. Kahneman. *Thinking, fast and slow*. macmillan, 2011.
- E. Karpas, O. Abend, Y. Belinkov, B. Lenz, O. Lieber, N. Ratner, Y. Shoham, H. Bata, Y. Levine, K. Leyton-Brown, D. Muhlgay, N. Rozen, E. Schwartz, G. Shachaf, S. Shalev-Shwartz, A. Shashua, and M. Tenenholz. Mrkl systems: A modular, neuro-symbolic architecture that combines large language models, external knowledge sources and discrete reasoning, 2022.
- W. Kim, A. Kanazaki, and M. Tanaka. Unsupervised learning of image segmentation based on differentiable feature clustering. *IEEE Transactions on Image Processing*, 29:8055–8068, 2020.
- T. Kipf, E. van der Pol, and M. Welling. Contrastive learning of structured world models. In *International Conference on Learning Representations*, 2020. URL <https://openreview.net/forum?id=H1gax6VtDB>.
- K. Kreutz-Delgado, J. F. Murray, B. D. Rao, K. Engan, T.-W. Lee, and T. J. Sejnowski. Dictionary Learning Algorithms for Sparse Representation. *Neural Computation*, 15(2):349–396, 02 2003. ISSN 0899-7667. doi: 10.1162/089976603762552951. URL <https://doi.org/10.1162/089976603762552951>.
- T. Kudo and J. Richardson. Sentencepiece: A simple and language independent subword tokenizer and detokenizer for neural text processing. *arXiv preprint arXiv:1808.06226*, 2018.
- B. M. Lake, R. Salakhutdinov, and J. B. Tenenbaum. Human-level concept learning through probabilistic program induction. *Science*, 350(6266):1332–1338, 2015.
- Y. LeCun. A path towards autonomous machine intelligence version 0.9. 2, 2022-06-27. *Open Review*, 62, 2022.
- B. Lefaudeux, F. Massa, D. Liskovich, W. Xiong, V. Caggiano, S. Naren, M. Xu, J. Hu, M. Tintore, S. Zhang, P. Labatut, and D. Haziza. xformers: A modular and hackable transformer modelling library. <https://github.com/facebookresearch/xformers>, 2022.
- T.-Y. Lin, P. Goyal, R. Girshick, K. He, and P. Dollár. Focal loss for dense object detection. In *Proceedings of the IEEE international conference on computer vision*, pages 2980–2988, 2017.
- Z. Lin, Y.-F. Wu, S. V. Peri, W. Sun, G. Singh, F. Deng, J. Jiang, and S. Ahn. Space: Unsupervised object-oriented scene representation via spatial attention and decomposition. *arXiv preprint arXiv:2001.02407*, 2020.
- P. R. Looockvane. *The Nature of Concepts: Evolution, Structure, and Representation*. New York: Routledge, 1999.
- C. Lou, W. Han, Y. Lin, and Z. Zheng. Unsupervised vision-language parsing: Seamlessly bridging visual scene graphs with language structures via dependency relationships. In *Proceedings of the IEEE/CVF Conference on Computer Vision and Pattern Recognition*, pages 15607–15616, 2022.
- Y. Ma, D. Tsao, and H.-Y. Shum. On the principles of parsimony and self-consistency for the emergence of intelligence. *Frontiers of Information Technology & Electronic Engineering*, 23(9):1298–1323, 2022.
- J. Mao, C. Gan, P. Kohli, J. B. Tenenbaum, and J. Wu. The neuro-symbolic concept learner: Interpreting scenes, words, and sentences from natural supervision. *arXiv preprint arXiv:1904.12584*, 2019.
- G. Mariani, I. Tallini, E. Postolache, M. Mancusi, L. Cosmo, and E. Rodolà. Multi-source diffusion models for simultaneous music generation and separation. *arXiv preprint arXiv:2302.02257*, 2023.
- L. Melas-Kyriazi, C. Rupprecht, I. Laina, and A. Vedaldi. Deep spectral methods: A surprisingly strong baseline for unsupervised semantic segmentation and localization. In *Proceedings of the IEEE/CVF Conference on Computer Vision and Pattern Recognition*, pages 8364–8375, 2022.

- J. A. Mendez and E. Eaton. How to reuse and compose knowledge for a lifetime of tasks: A survey on continual learning and functional composition, 2022.
- J. A. Mendez, H. van Seijen, and E. EATON. Modular lifelong reinforcement learning via neural composition. In *International Conference on Learning Representations*, 2022. URL <https://openreview.net/forum?id=5XmLzds1FNN>.
- F. Milletari, N. Navab, and S.-A. Ahmadi. V-net: Fully convolutional neural networks for volumetric medical image segmentation. In *2016 fourth international conference on 3D vision (3DV)*, pages 565–571. Ieee, 2016.
- P. Min. binvox. <http://www.patrickmin.com/binvox> or <https://www.google.com/search?q=binvox>, 2004–2019. Accessed: yyyy-mm-dd.
- A. Newell and H. A. Simon. Computer science as empirical inquiry: Symbols and search. *Commun. ACM*, 19(3): 113–126, mar 1976. ISSN 0001-0782. doi: 10.1145/360018.360022. URL <https://doi.org/10.1145/360018.360022>.
- F. S. Nooruddin and G. Turk. Simplification and repair of polygonal models using volumetric techniques. *IEEE Transactions on Visualization and Computer Graphics*, 9(2):191–205, 2003.
- A. Odena, V. Dumoulin, and C. Olah. Deconvolution and checkerboard artifacts. *Distill*, 2016. doi: 10.23915/distill.00003. URL <http://distill.pub/2016/deconv-checkerboard>.
- OpenAI. Ppo2. <https://stable-baselines.readthedocs.io/en/master/modules/ppo2.html> , 2018-2021.
- K. Papineni, S. Roukos, T. Ward, and W.-J. Zhu. Bleu: a method for automatic evaluation of machine translation. In *Proceedings of the 40th annual meeting of the Association for Computational Linguistics*, pages 311–318, 2002.
- L.-A. Petitto. How the brain begets language. *The cambridge companion to chomsky*, pages 84–101, 2005.
- A. Radford, J. W. Kim, C. Hallacy, A. Ramesh, G. Goh, S. Agarwal, G. Sastry, A. Askell, P. Mishkin, J. Clark, et al. Learning transferable visual models from natural language supervision. In *International conference on machine learning*, pages 8748–8763. PMLR, 2021.
- R. Ramesh and P. Chaudhari. Model zoo: A growing brain that learns continually. In *International Conference on Learning Representations*, 2022. URL <https://openreview.net/forum?id=WfvgGBcgbE7>.
- R. Riegel, A. Gray, F. Luus, N. Khan, N. Makondo, I. Y. Akhalwaya, H. Qian, R. Fagin, F. Barahona, U. Sharma, et al. Logical neural networks. *arXiv preprint arXiv:2006.13155*, 2020.
- G. Rizzolatti. The mirror neuron system and its function in humans. *Anatomy and embryology*, 210(5-6):419–421, 2005.
- G. Rizzolatti, L. Fadiga, V. Gallese, and L. Fogassi. Premotor cortex and the recognition of motor actions. *Cognitive brain research*, 3(2):131–141, 1996.
- R. Rombach, A. Blattmann, D. Lorenz, P. Esser, and B. Ommer. High-resolution image synthesis with latent diffusion models. In *Proceedings of the IEEE/CVF Conference on Computer Vision and Pattern Recognition (CVPR)*, pages 10684–10695, June 2022.
- T. Schick, J. Dwivedi-Yu, R. Dessì, R. Raileanu, M. Lomeli, L. Zettlemoyer, N. Cancedda, and T. Scialom. Toolformer: Language models can teach themselves to use tools, 2023.
- J. Schulman, F. Wolski, P. Dhariwal, A. Radford, and O. Klimov. Proximal policy optimization algorithms. *arXiv preprint arXiv:1707.06347*, 2017.
- M. H. Segler, M. Preuss, and M. P. Waller. Planning chemical syntheses with deep neural networks and symbolic ai. *Nature*, 555(7698):604–610, 2018.
- M. Shanahan, K. Nikiforou, A. Creswell, C. Kaplanis, D. Barrett, and M. Garnelo. An explicitly relational neural network architecture. In *International Conference on Machine Learning*, pages 8593–8603. PMLR, 2020.
- Y. Song, J. Sohl-Dickstein, D. P. Kingma, A. Kumar, S. Ermon, and B. Poole. Score-based generative modeling through stochastic differential equations. In *International Conference on Learning Representations*, 2021. URL <https://openreview.net/forum?id=PxtTIG12RRHS>.
- J. Sun, H. Sun, T. Han, and B. Zhou. Neuro-symbolic program search for autonomous driving decision module design. In *Conference on Robot Learning*, pages 21–30. PMLR, 2021.
- T. Taniguchi, T. Nagai, T. Nakamura, N. Iwahashi, T. Ogata, and H. Asoh. Symbol emergence in robotics: a survey. *Advanced Robotics*, 30(11-12):706–728, 2016.
- T. Taniguchi, E. Ugur, M. Hoffmann, L. Jamone, T. Nagai, B. Rosman, T. Matsuka, N. Iwahashi, E. Oztop, J. Piater, et al. Symbol emergence in cognitive developmental systems: a survey. *IEEE transactions on Cognitive and Developmental Systems*, 11(4):494–516, 2018.

- M. Tomasello. *Origins of Human Communication*. The MIT Press, 08 2008. ISBN 9780262285070. doi: 10.7551/mitpress/7551.001.0001. URL <https://doi.org/10.7551/mitpress/7551.001.0001>.
- W. Van Gansbeke, S. Vandenhende, S. Georgoulis, and L. Van Gool. Unsupervised semantic segmentation by contrasting object mask proposals. In *Proceedings of the IEEE/CVF International Conference on Computer Vision*, pages 10052–10062, 2021.
- A. Vaswani, N. Shazeer, N. Parmar, J. Uszkoreit, L. Jones, A. N. Gomez, L. Kaiser, and I. Polosukhin. Attention is all you need. *Advances in neural information processing systems*, 30, 2017.
- M. Vlastelica, M. Rolinek, and G. Martius. Neuro-algorithmic policies enable fast combinatorial generalization. In M. Meila and T. Zhang, editors, *Proceedings of the 38th International Conference on Machine Learning*, volume 139 of *Proceedings of Machine Learning Research*, pages 10575–10585. PMLR, 18–24 Jul 2021. URL <https://proceedings.mlr.press/v139/vlastelica21a.html>.
- P.-W. Wang, P. Donti, B. Wilder, and Z. Kolter. Satnet: Bridging deep learning and logical reasoning using a differentiable satisfiability solver. In *International Conference on Machine Learning*, pages 6545–6554. PMLR, 2019.
- J. C. Whittington, T. H. Muller, S. Mark, G. Chen, C. Barry, N. Burgess, and T. E. Behrens. The tolman-eichenbaum machine: unifying space and relational memory through generalization in the hippocampal formation. *Cell*, 183(5): 1249–1263, 2020.
- B. Wicker, C. Keysers, J. Plailly, J.-P. Royet, V. Gallese, and G. Rizzolatti. Both of us disgusted in my insula: the common neural basis of seeing and feeling disgust. *Neuron*, 40(3):655–664, 2003.
- T. Wu, M. Tjandrasuwita, Z. Wu, X. Yang, K. Liu, R. Sasic, and J. Leskovec. Zeroc: A neuro-symbolic model for zero-shot concept recognition and acquisition at inference time. *Advances in Neural Information Processing Systems*, 35:9828–9840, 2022.
- Z. Wu, Y. Xiong, S. X. Yu, and D. Lin. Unsupervised feature learning via non-parametric instance discrimination. In *Proceedings of the IEEE conference on computer vision and pattern recognition*, pages 3733–3742, 2018.
- H.-M. Yang, X.-Y. Zhang, F. Yin, and C.-L. Liu. Robust classification with convolutional prototype learning. In *Proceedings of the IEEE conference on computer vision and pattern recognition*, pages 3474–3482, 2018.
- H. Young, O. Bastani, and M. Naik. Learning neurosymbolic generative models via program synthesis. In *International Conference on Machine Learning*, pages 7144–7153. PMLR, 2019.
- C. Yu, X. Zhu, X. Zhang, Z. Wang, Z. Zhang, and Z. Lei. Hp-capsule: Unsupervised face part discovery by hierarchical parsing capsule network. In *Proceedings of the IEEE/CVF Conference on Computer Vision and Pattern Recognition (CVPR)*, pages 4032–4041, June 2022.
- A. Ziegler and Y. M. Asano. Self-supervised learning of object parts for semantic segmentation. In *Proceedings of the IEEE/CVF Conference on Computer Vision and Pattern Recognition*, pages 14502–14511, 2022.

A Detailed Related Works

In this work, we discover the process of symbolic knowledge that emerged from neural knowledge through a self-supervised learning of the predicate transitional representation, which is related to the following disciplines.

A.1 Symbol Emergence

Symbol emergence Taniguchi et al. [2018, 2016] researches how symbolic knowledge are emerged in natural and artificial cognitive systems. It relates to the idea of learning world model LeCun [2022]. In this work, we care about the neural foundation that how it happens in NN that is based on highly distributed and dynamic representations.

Symbolic intelligence has long been a key topic in cognitive science and neural science Whittington et al. [2020]. The symbols continuously evolve from human social and environmental interactions. A critical view assumes that the symbolic representation in human emerges before social communication under evolutionary pressure from internal computations and communications in the brain Taniguchi et al. [2018] which support us to learn a transitional representation without phylogenetic processes Ma et al. [2022] while symbolic representation is highly socialized. Mirror neurons have been regarded as a candidate for the neural emergence of action concepts Rizzolatti [2005], Di Pellegrino et al. [1992], Gallese et al. [2009], Rizzolatti et al. [1996]. Where brain imaging evidence has also shown that primitive concepts related to objects, events, actions, feelings, etc. exist in different mirror systems Wicker et al. [2003]. Language evolution theory Arbib [2002], Petitto [2005], Lockvane [1999] claims that such mirror systems form a foundation that combined with a recursive structure of action planning and imitation pushes the emergence of language. And the mirror system activity has been detected in or near Broca’s area, the area recognized for processing languages Arbib [2011], Tomasello [2008], Higuchi et al. [2009].

The studies of the mirror systems support the idea that the prehuman brain emerges as basic symbols for rudimentary planning and decision-making, and those symbols rapidly evolved once externalized through communications and pave the way for the creation of language Taniguchi et al. [2018]. It supports the existence of a transition stage between neural representations and human symbolic knowledge that emerged through interaction with the environment before human communications happen, which inspires us to emulate such an evolution process of a rudimentary transitional representation with self-supervised learning.

A.2 Neural-Symbolic AI

One emerging research area that tries to bridge the power of machine learning and the classic symbolic AI thus combining System I and System II intelligence is Neural-Symbolic AI (NSAI) Garcez and Lamb [2023]. NSAI is a tremendously broad concept whose definition and coverage are still vague, we roughly conclude the existing methods into two streams:

1) Specialized NSAI that tries to introduce the symbolic method to NN for solving a specific problem. Segler et al. [2018] combines Monte Carlo tree search with symbolic AI for learning retrosynthetic routes in small organic molecule synthesis. Amizadeh et al. [2020] uses a differentiable First-Order-Logic (FOL) reasoner for the Visual Question Answering (VQA) problem. Sun et al. [2021] designed a Neural-Symbolic Program Search (NSPS) that synthesizes programs for controlling autonomous vehicles. Young et al. [2019] applied a symbolic controller in a generative model for generating the images with looped patterns. Inala et al. [2020] synthesizes control policy for multi-agent communication by a transformer policy network and a program synthesizer. The specialized methods suffer from ad-hoc solutions which makes it hard to transfer the method from one task to another. This problem is also shown in many general NSAI methods as they made strict assumptions about the methods. Our method focuses on representation and can transfer to the general case with a transfer learning paradigm which has been proven to be extremely successful in today’s deep learning.

2) General NSAI that tries to explore a general method or fundamental insights of combining NN and symbolic methods for solving general problems. Wang et al. [2019] relaxed SAT problem and proposed a differentiable solver as a NN layer. Riegel et al. [2020] relaxed FOL propositions as NN layers. Cornelio et al. [2023] introduced a symbolic reasoner to correct the structural error made by an attention-enhanced predictor. Dong et al. [2019] uses NN as trainable logical functions in logical programming. Dai et al. [2019] proposed abductive learning to optimize the NN with logical programs. Goyal et al. [2021] designed neural production systems that learn entities and related knowledge in the visual environment. Vlastelica et al. [2021] uses blackbox-differentiation to train a neural-algorithmic module. Karpas et al. [2022] and Schick et al. [2023] apply prompt tuning to enable language models call symbolic modules. Existing methods focus on the reasoning side while ignoring the problem of good representation for NSAI which makes them hard to scale and it is a major concern in this work.

A.3 Compositional Learning

Compositional machine learning learns and uses compositional knowledge to achieve System II intelligence. Hinton [2021] proposed an architecture to represent part and whole hierarchy inside NN, Garau et al. [2022] extended this idea with an attention model. Du et al. [2020] uses Energy-Based Models (EBM) to generate images that are composed of basic concepts. Chen et al. [2020] learn to compose complex programs with basic programs. Mendez et al. [2022] learns reusable compositions for life-long learning, and Mendez and Eaton [2022] gives a comprehensive survey on compositional life-long learning.

Concept learning A more specific area that focuses on compositional representation is concept learning. Lake et al. [2015] learns to represent new concepts in handwritten characters with primitives by Bayesian Program Learning. Shanahan et al. [2020] uses attention to learn relations among objects. Mao et al. [2019] learns visual concepts as embeddings while Cao et al. [2021] learns them as prototypes. Kipf et al. [2020] learns concepts by contrastive learning and represents relation with an implicit graph. Wu et al. [2022] embeds concepts and relations with EBMs and then applies the EBM for zero-shot inference, Du et al. [2021] also uses EBM to represent concepts. LeCun [2022] introduced an EBM-based framework that implicitly learns hierarchical reasoning. Compared to the above methods, our method gives a general framework for learning arbitrary predicates without any supervision or prior knowledge.

A.4 Unsupervised Segmentation and Parsing

Segmentation and parsing convert high-dimensional data into a structural representation that implements a neural-symbolic transition. How to learn them in an unsupervised way is a challenging problem. Lin et al. [2020] uses spatial attention to learn scene parsing. Bear et al. [2020] learns to parse the scene with physical properties. Kim et al. [2020] learns image segmentation unsupervisedly with clustering on features whereas Van Gansbeke et al. [2021] also applies clustering on a contrastive learning method for semantic segmentation. Lou et al. [2022] learns to parse image-caption pair into a parse graph unsupervisedly by an alignment between scene graph and dependency graph Melas-Kyriazi et al. [2022] learns unsupervised semantic segmentation with deep spectral methods. These methods do not learn the hierarchical and compositional concepts in parsing which are considered in the co-part segmentation methods.

Co-part segmentation Co-part segmentation learns to decompose an image into visual parts. Collins et al. [2018] segment image into visual concepts by NMF. Hung et al. [2019] and Choudhury et al. [2021] learns the co-part segmentation by self-supervised learning. Amir et al. [2021] extracts pre-trained Vision Transformer (ViT) features for co-part segmentation. Gao et al. [2021] learns co-parts by making use of the motion information in videos. Ziegler and Asano [2022] learns part features for semantic segmentation with a Sinkhorn-Knopp clustering which has been applied by Caron et al. [2020]. Yu et al. [2022] utilizes the capsule networks to discover the face parts. He et al. [2022] learns part segmentation through a hierarchical image generation process. The above methods largely rely on visual features or categories prior and ad-hoc to vision thus hard to extend to the general case of symbolic representations compared to our method.

B Method details

We provide the details of our proposed method, including the detailed model architecture design, the loss functions, and more insights about how the method work, including the relation prediction and symbol grounding.

B.1 Model details

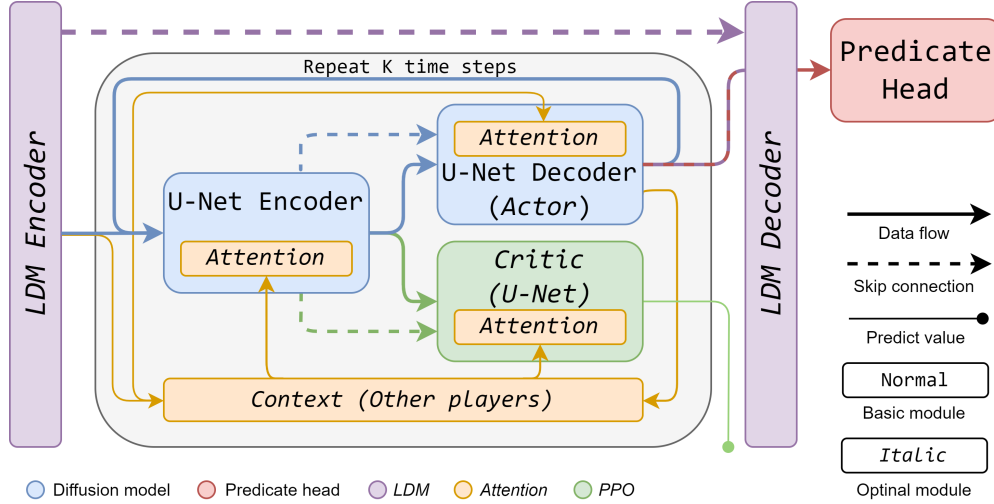


Figure 4: Illustration of the model architecture. Our model is highly modular. Blocks with italic font are optional optimizations. Different color marks the information flow of the 5 different modules.

The architecture of our model is shown in Figure 4, our model contains 2 basic modules, diffusion model, predicate head, and 3 optional optimizations, LDM, attention, and PPO. The architecture is highly modularized, apart from the diffusion model backbone, optional modules and predicate head are “plug-and-play”, which means removing any of them, the model can still work. One can config the model for different needs and scenarios.

Each module corresponds to a different function. The diffusion model is the backbone for implementing the game-theory-inspired decomposition. The predicate head is the core of learning transitional representation and can be agnostic to the architecture which means theoretically one can put it on the top of any model for learning the transitional representation. The PPO module is to introduce heuristics and human knowledge. LDM module is to improve efficiency. And attention module is designed to introduce context information, in our work, we simply apply other players as context, while in other diffusion model work Rombach et al. [2022], the context has been used to introduce multimodal inputs. We provide detail of each module here. For simplicity, we assume single 2D input, and it can be easily extended for batch input and 3D input.

B.1.1 Diffusion model

Algorithm 1 Decompose an input

Require: an actor model $Actor(\cdot, \cdot; \theta_A, D)$, decoder $f_g: \mathbb{R}^{dim_r} \mapsto \mathbb{R}^{H \times W \times C}$

Require: an input $x \in \mathbb{R}^{H \times W \times C}$, number of players N , time steps K

- 1: Randomly initialize variables of N players $\vec{r}(0) \in \mathbb{R}^{N \times dim_r}$
 - 2: Initialize player id embedding $\vec{e}_{pid} \in \mathbb{R}^{N \times d_{emb}}$ and time embedding $\vec{e}_{time} \in \mathbb{R}^{K \times d_{emb}}$
 - 3: **for** $t \in \{1, \dots, K\}$ **do**
 - 4: $\vec{x}(t) = f_g(\vec{r}(t))$, where $\vec{x}(t) \in \mathbb{R}^{N \times H \times W \times C}$ ▷ visual parts of N players
 - 5: $\forall j \in \{1, \dots, N\}, s^j(t) = [x; x^j(t); \sum_{k \neq j} x_i^k(t); \sum_{k \neq j, d \in D_2} P(x_i^k(t), d | x_i^j(t)) x_i^k(t)]$
 - 6: $\vec{e}_{inp}(t) = \vec{e}_{pid} + e_{time}^t + GetPrediEmb(\vec{s}(t), D)$ ▷ see B.1.2 for $GetPrediEmb$
 - 7: $\vec{r}(t+1) = Actor(\vec{s}(t), \vec{e}_{inp}(t); \theta_A, D)$
 - 8: **end for**
 - 9: **return** $\vec{r}(K)$
-

The backbone of our model is a *diffusion model* utilizing the architecture from SMLD Song et al. [2021], SMLD is based on U-Net, U-Net is a symmetric encoder-decoder structure that an encoder iteratively downsample the sample with convolutional layers, the decoder iteratively upsamples the encoder output by interpolation and convolution layers with skip connections from the encoder. Algorithm 1 shows how the model decomposes an input.

Between each convolution layer in U-Net, SMLD introduces a dense layer to bring in the time step embedding $e_{time} \in \mathbb{R}^{d_{emb}}$ by adding the output of this dense layer to the output of the convolutional layer. Every time step t , for a player j , the model accepts two terms as input, the input state $s_t^j \in \mathbb{R}^{H \times W \times C_{inp}}$ and embedding $e_{inp}(t) \in \mathbb{R}^{d_{emb}}$, and output an updated decomposed composition $x^j(t+1)$.

Input Embedding In addition to the time step embedding, we additionally input a *predicate embedding* $e_{predi}(t)$ that is computed every time step t after the broadcast and a *player id embedding* e_{pid} that is provided during initialization. We add them to time step embedding similar to BERT Devlin et al. [2019] that adds up different embeddings as $e_{inp}(t) = e_{time} + e_{predi}(t) + e_{pid}$.

Predicate embedding is computed with the predicate head which will be discussed in B.1.2. The player id embedding is randomly chosen from an embedding layer $E_{pid} \in \mathbb{R}^{N_{pid} \times d_{emb}}$ for each player every time, where N_{pid} is a relatively large number compared to the number of players N .

Input state For a player j , The input state every time step is a channel-wise stack of multiple feature maps including the input image $x \in \mathbb{R}^{H \times W \times C}$, current composed result $x^j(t)$, a competitors map $\sum_{k \neq j} x^k(t)$ that described the positions that are already occupied by the competitors and a cooperator map that computed with the predicate head which will be discussed in B.1.2.

B.1.2 Predicate head

Algorithm 2 Compute clustering error for 1 and 2-ary predicates

Require: variables $\vec{r} \in \mathbb{R}^{m \times dim_r}$, prototypes $D_1 \in \mathbb{R}^{N_{D_1} \times dim_m}$, $D_2 \in \mathbb{R}^{N_{D_2} \times dim_m}$

Require: memory banks $M_1 \in \mathbb{R}^{L_1 \times dim_m}$, $M_2 \in \mathbb{R}^{L_2 \times dim_m}$

Require: mappers $f_{m_1}, f_{m_2} : \mathbb{R}^{dim_r} \mapsto \mathbb{R}^{dim_m}$, decoder $f_g : \mathbb{R}^{dim_r} \mapsto \mathbb{R}^{H \times W \times C}$

Require: distance metric $d : \mathbb{R}^{n_1 \times dim_m} \times \mathbb{R}^{n_2 \times dim_m} \mapsto \mathbb{R}^{n_1 \times n_2}$

```

1:  $\vec{x} = filter(f_g(\vec{r}))$ , where  $\vec{x} \in \mathbb{R}^{m' \times H \times W \times C}$  ▷ filter out unwanted visual parts
2:  $\vec{m}_1 = sample(f_{m_1}(\vec{x}), N_{m_1})$ , where  $\vec{m}_1 \in \mathbb{R}^{N_{m_1} \times dim_m}$  ▷ random sample  $N_{m_1}$  items
3:  $\vec{p} = filter(\{x^q + x^w, \forall x^q, x^w \in \vec{x}\})$ , where  $\vec{p} \in \mathbb{R}^{m'' \times H \times W \times C}$  ▷ pair representations
4:  $\vec{m}_2 = sample(f_{m_2}(\vec{p}), N_{m_2})$ , where  $\vec{m}_2 \in \mathbb{R}^{N_{m_2} \times dim_m}$  ▷ random sample  $N_{m_2}$  items
5:
6: function ASSIGN( $C'_i, D_i$ )
7:    $\vec{C} = \{ \frac{\sum_{0 < j \leq N_{m_i}} D_i^j \mathbb{1}(C_i^j == k)}{\sum_{0 < j \leq N_{m_i}} \mathbb{1}(C_i^j == k)}, \forall 0 < k \leq N_{D_i} \}$  ▷ Centroids for each cluster
8:    $d_E = L1\_Dist(\vec{C}, \mathbb{I}_{N_{D_i}})$ ,  $d_E \in \mathbb{R}^{N_{D_i} \times N_{D_i}}$  ▷ L1 Distance from centroids to permutations of assignments
9:   while  $k < N_{D_i}$  do
10:      $(row, col) = argmin(d_E)$ 
11:      $Y_i^k = col$ 
12:      $d_E[row, :] = +inf$ 
13:      $d_E[:, col] = +inf$ 
14:   end while
15:   return  $Y_i$ 
16: end function
17:
18: function GETLOSS( $\vec{m}_i, M_i, D_i$ )
19:    $C_i = K-Means([\vec{m}_i; M_i])$ ,  $C_i^j = \{C_i^j, j = \{1, \dots, N_{m_i}\}\}$ 
20:    $Y_i = Assign(C_i^j, D_i)$ ,  $Y_i \in \mathbf{Z}^{N_{m_i} \times N_{D_i}}$ 
21:    $dist_i = d(\vec{m}_i, D_i)$ ,  $dist_i \in \mathbb{R}^{N_{m_i} \times N_{D_i}}$ 
22:   return  $CrossEntropyLoss(dist_i, E_i)$ 
23: end function
24: return  $GetLoss(\vec{m}_1, M_1, D_1) + GetLoss(\vec{m}_2, M_2, D_2)$ 

```

The *predicate head* is the core of our model for learning transitional representation, it embeds the decomposed compositions to a latent space and clusters them to learn the dictionaries for transitional representation. Our predicate head contains a shared mapper f_{mapper} implemented as convolution layers and a global pooling for all dictionaries that map compositions $\vec{x} \in \mathbb{R}^{m \times H \times W \times C}$ to tensors $\vec{r} \in \mathbb{R}^{m \times d_{mapper}}$, and multiple predicate dictionaries for predicates

of different arity and order, each dictionary composed of a linear layer for query $Q \in \mathbb{R}^{d_{\text{mapper}} \times \text{dim}_m}$, prototypes $D \in \mathbb{R}^{N_D \times \text{dim}_m}$ for storing dictionary terms, and memory bank $M \in \mathbb{R}^{L \times \text{dim}_m}$. Specifically, in our work, we apply the multi-prototype Yang et al. [2018], which means for each dictionary term, we store K_D prototypes, a multi-prototype dictionary is $D \in \mathbb{R}^{K_D \times N_D \times \text{dim}_m}$.

In each time step t , for player j , the predicate head accepts the current decomposition $x^j(t)$ as input and outputs the predicate embedding and cooperator map. After K time steps, given the representation \vec{r} , the predicate head computes the clustering error by Algorithm 2.

We further explore a **Higher-Order Logic (HOL)** predicate, a HOL representation is given by dot-product attention, as $h_i^j = \sum_{k \neq j} P(r_i^j, r_i^k) r_i^k$, and HOL pairs $g_i^{q,w}$ can be constructed with h_i in the same way to 2-ary predicates by summing up the corresponding image parts.

Predicate embedding For a player j , the predicate embedding is computed as $e_{\text{predi}}^j(t) = \sum_{d \in D_1} P(d|x^j(t))d$ where $P(d|x^j(t)) \propto -\text{dist}(d, q_1^j(t))$, dist is a distance metric, we use L2 distance by default in this work, and $q_1^j(t) = Q_1 f_{\text{mapper}}(x^j(t))$. It represents the potential 1-ary predicate of the current decomposition result.

If using a higher-order predicate, we sum $e_{\text{predi}}^j(t)$ with $\sum_{d \in D_{h1}} P(d|h^j(t))d$, where $P(d|h^j(t)) \propto -\text{dist}(d, q_{h1}^j(t))$, $q_{h1}^j = Q_{h1} f_{\text{mapper}}(f_g(h^j(t)))$ and $h^j(t) = \sum_{k \neq j} P(r^j, r^k) r^k$ where $P(r^j, r^k) \propto r^j r^k$, the dot-product distance, to cover a higher-order predicate over grouped players.

Cooperator map The cooperator map computed as $\sum_{k \neq j, d \in D_2} P(x^k(t), d|x^j(t))x^k(t)$, the positions that may form a 2-ary relationship with the player, where $P(x^k(t), d|x^j(t)) \propto -\text{dist}(d, q_1^{(j,k)})$, $q_1^{(j,k)} = Q_1 f_{\text{mapper}}(f_g(x^k(t) + x^j(t)))$, and dist is a distance metric, in our work, we use L2 distance by default.

When the higher-order predicate is used, the cooperator map will channel-wise stack with $\sum_{k \neq j, d \in D_{h2}} P(h^k(t), d|h^j(t))x^k(t)$ which represents the pairs of groups, where $P(h^k(t), d|h^j(t)) \propto -\text{dist}(d, q_{h2}^{(j,k)})$, $q_{h2}^{(j,k)} = Q_{h2} f_{\text{mapper}}(f_g(h^k(t)) + f_g(h^j(t)))$, dist and h are the same above.

B.1.3 Latent Diffusion Model

LDM Rombach et al. [2022] uses an Auto-Encoder to encode an input $x \in \mathbb{R}^{H \times W \times C}$ to a compressed input $x' \in \mathbb{R}^{H' \times W' \times C'}$, where $H' < H$ and $W' < W$, and input the compressed input x' instead of the original input x to the diffusion model, which outputs the composition $x^{j'} \in \mathbb{R}^{H' \times W' \times C'}$ in latent space, then use the decoder to decompress it to the original pixel space $x^j \in \mathbb{R}^{H \times W \times C}$.

We use a U-Net-based Auto-Encoder in our work, and we keep the skip connection that inputs the downsampled middle results from the encoder to the decoder.

B.1.4 Attention layers

We introduce optional transformer blocks Vaswani et al. [2017] between the convolutions layers in U-Net similar to CLIP Radford et al. [2021]. There are two types of transformer blocks have been used in our methods, self-attention, and cross-attention, while self-attention is only used in the encoder part when using an LDM since there is no context, and all other places use the cross-attention. For cross-attention, the context is the set of the mapped representation of competitors $\{\tau_1, \tau_2, \dots, \tau_{j-1}, \tau_{j+1}, \dots, \tau_m\}$. We utilize the memory-efficient attention in xFormers Lefaudeux et al. [2022] in our implementation.

Attention also gives a powerful tool for incorporating multimodal information Cheng et al. [2021b] and inductive biases Cheng et al. [2021a], the context may come from other modalities, similar to Rombach et al. [2022], and in a multi-agent case, the context could come from other agents.

B.1.5 PPO and Actor-Critic

PPO Schulman et al. [2017] uses an Actor-Critic framework to train the agent, we apply a shared encoder actor and critic that the U-Net encoder in the diffusion model is shared, and we train two decoders for the actor and critic respectively. The actor samples a move with a Bernoulli distribution, where the probability is given by the diffusion model output, on each pixel as a mask. A reward function rating on this mask by the loss and the shape score. And the critic is trained to predict the reward given a state.

We follow the PPO algorithm with PPO2 implementation OpenAI [2018-2021]. The model is updated every few steps of sampling. A small buffer that saves actions, states, following states, and several other useful information about recent samples is maintained and iteratively retrieved when updating the model.

B.2 Mechanism Design and GT Loss

Here, we provide details of the mechanism design of our game-theory-based decomposition. The mechanism design largely influences the self-organization of the players and the equilibrium state, thus we need to design a fair game for ensuring the model reaches a desired equilibrium. We first introduce the detail of the GT loss which decides the “rules” of the game, then we discuss the unwanted cases in the game and the solutions we use to handle them.

B.2.1 Loss function detail

As given by Formula 4, the GT loss is composed of four terms, we give detail for each of them:

Reconstruction loss $L_{Reconstruction}$ reconstruction term requires the players to corporately reconstruct the input which is computed as a reconstructed error between the reconstructed input by all players $\tilde{x} = \sum_j x^j$ and the input x . The reconstruction error can be measured in many ways like the Mean Absolute Error (MAE), Mean Squared Error (MSE), in this work, we applied a combination of focal loss Lin et al. [2017] and dice loss Milletari et al. [2016] which can alleviate the imbalance class problem as the reconstruction error.

Overlapping loss $L_{overlap}$ with only cooperation, the game may easily converge to the case that all players output the same result (i.e. the reconstructed input), thus essentially no cooperation at all. Thus, we introduce the competition between players that avoid overlap between the outputs by $\min_{\theta} \max(0, \tilde{x} - x)$, which penalizes the exceeded parts of the reconstructed input. The term can be seen as a global resource limitation.

Resources loss $L_{resources}$ We observe that by introducing the competition, the model can converge to another extreme where only one player outputs and reconstructed the input, and all other players give empty output. We solve this problem by introducing a resources mechanism in that every player has a limited quota q_R , and we define the resources used by a player as the L1 norm of the output, we restrict each player to avoid exceeding their resource limitation by $\min_{\theta} \sum_j \max(0, q_R - |x^j|)$. This term requires the players to compete and cooperate, while we may adjust the balance between them by adjusting the quota.

L2 Norm L_{norm} Another problem comes to the action space of the players, which can be restricted by the L2 norm of an unactivated output \bar{x}^j , where $x^j = Sigmoid(\bar{x}^j)$. Since the pixels are normalized between 0 and 1, and the effective input range for a Sigmoid function is between around -6 and 6. Thus, values that far are beyond this range are meaningless because the activation is already saturated. So we introduce an L2 norm to the unactivated output as $\min_{\theta} \sum_j \|\bar{x}^j\|_2^2$.

The four terms ensure an environment that forces the players to find a good way to compete and cooperate with each other by restricting the global resources from the input through the overlapping term and the resources each player has by resources term, to finish a common goal of reconstructing the input. While the norm term gives a reasonable action range for each player so that the players do not need to be stuck on a huge unrelated area.

B.2.2 Handling unwanted cases

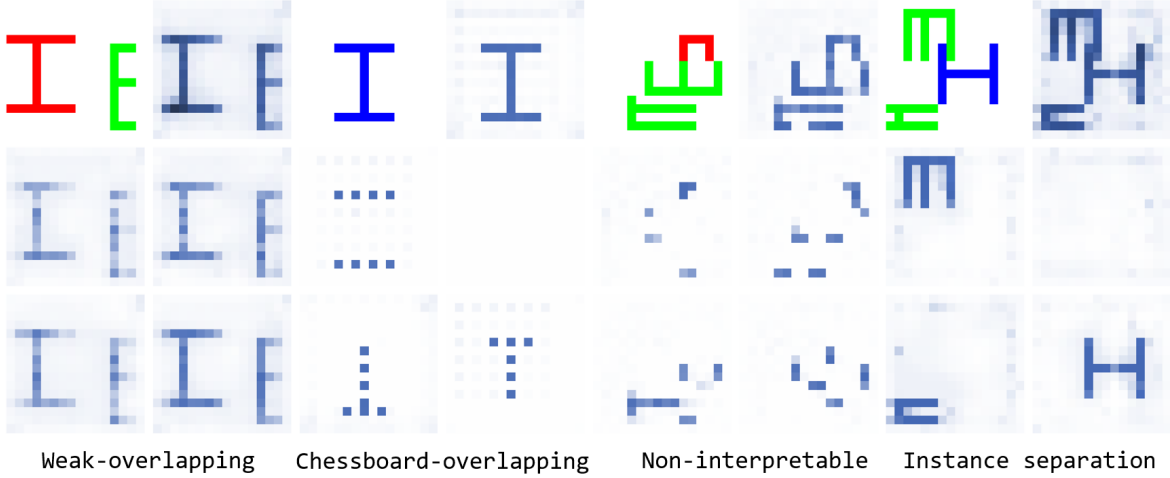


Figure 5: Unwanted cases were shown during our mechanism design. The first row shows pairs of input (left) and reconstructed result (right), and the remaining rows are the outputs of players. Another two common cases not shown here are all players output the same output and one player output while all others are empty.

GT loss only gives a fair environment for the game, there are still other unwanted cases that need to be handled with additional techniques which are shown in Figure 5. The **weak-overlapping** is a tricky way learned by the model to bypass the mechanisms. It means each player outputs a weak copy of the input $x^j = cx$ where $0 < c < 1$, it fully meets the requirements from the GT loss. We solve it with a **soft step function** trick, which computing the overlapping loss by $\max(0, \sum_j \text{Step}(x^j; th_S) - \text{Step}(x; th_S))$, where Step is a point-wise step function that assigns 1 to a position if the value above a threshold th_S and 0 otherwise. A soft step function can be implemented with a Heaviside function. With a step function, the overlapping loss becomes more sensitive and a small value in a position will be regarded as an occupation. And the threshold controls the sensitivity. Thus the model cannot cheat with weak overlapping and be more careful in assigning values.

Another interesting situation is **chessboard overlapping**, where the players avoid overlap by outputting pixels with intervals. While this actually only happens when we use the deconvolutional layer as an upsampling technique in our U-Net decoder. Thus a simple way to avoid this case is by avoiding using a deconvolutional upsampling which suffers from the checkerboard artifact Odena et al. [2016]. However, it also drives us to think about what would be a fundamental way to solve such a case since a simple specialized solution may not always exist. One way to alleviate it could be our shape score or essentially the principle of least effort since the shape score is designed to find the natural shapes that can be easily used or produced, and such segmented shapes seem to be hard to apply in real life and unlikely to emerge in the natural development of cognition.

The **non-interpretable** shape happens in a base model without a predicate head, by applying a predicate clustering and other techniques that encourage interpretability, such cases can largely be reduced. And the **instance separation** is a very interesting case in that the model learns an unwanted good case that gives a segmentation of instances, which shows the great potential of the proposed method and the power of *self-organization*. We hypothesized that this case is caused by a large dictionary size and a large batch size, thus bringing about a scenario similar to SWaV Caron et al. [2020] which learns an object-level dictionary.

B.3 Hierarchical Concepts and Relation Clustering

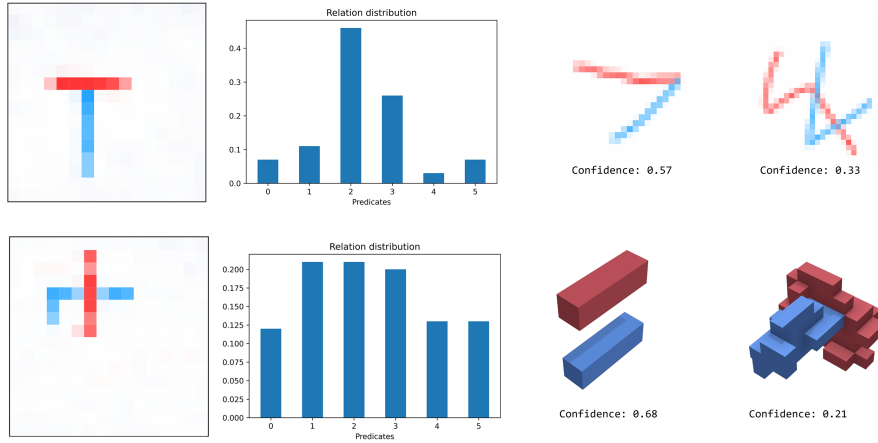


Figure 6: Illustration of a relation clustering in the three datasets.

We give more insights on how relation clustering or the 2-ary predicates work here. In Figure 6, we show examples from the three datasets, we query a pair of a red and a blue part in the learned 2-ary predicate dictionary by comparing the distance of their representation obtained by the mapper and query layer and the 2-ary predicate prototypes, which gives a distribution of the confidence over each predicate, or a relative distance to them. One can also use an absolute distance with a threshold to get better Out-Of-Distribution (OOD) detection ability for not only the relation prediction but also other dictionaries and also better robustness Yang et al. [2018], for simplicity, we keep a relative distance in our work.

On the left side of the figure, we visualized the distribution in two LineWorld samples, where a more common “T” pattern is close to predicate 3, while another overlapping pattern that is not allowed in the dataset is remote to all prototypes. On the right side, we provide the confidence of the predicate with the largest confidence for each sample, we can see that the more common sample shows higher confidence than a more random one which is hard to be concluded as any categories.

While the 1-ary predicates learn visual primitives, the 2-ary predicates implicitly learn the common combinations, and higher-ary and order predicates can be seen as learning subparts. It shows that our method can implicitly learn the **hierarchical concepts** Lake et al. [2015] which is claimed as a key for achieving human intelligence.

B.4 Symbol Grounding

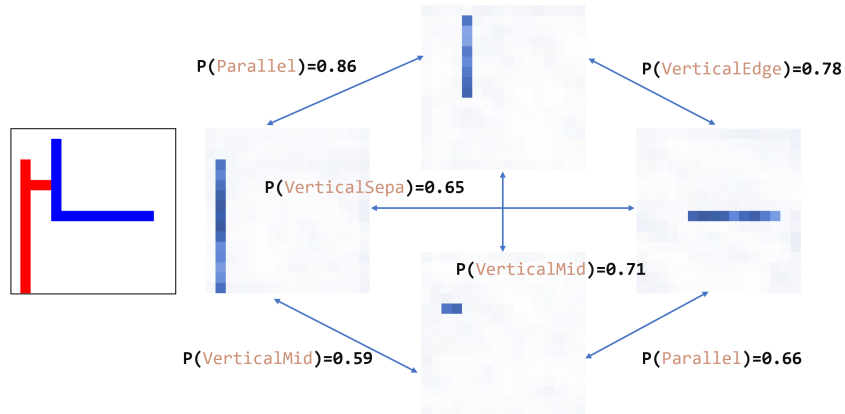


Figure 7: Illustration of the symbol ground of an LW-G sample. Empty players are omitted.

Here, we show how the symbol grounding work that grounds an image to a set of predefined predicates. Figure 7 shows an example of grounding an LW-G sample to the predicates defined by the babyARC engine. The model first decomposes the image into parts, which are the lines in different positions with different lengths, as the 1-ary predicates. Then predict the relationships between the pairs of the parts by the relation predictor which is implemented as 2-ary predicate prototypes.

This gives a complete graph G_S with 1-ary concepts as nodes and 2-ary relationships as edges. Suppose the ground-truth graph is G_{gt} . Since the number of players is assumed to be larger than the number of ground-truth concepts, the model actually gives a complete graph with outputs from all players as nodes G_P , and we require G_{gt} to be a sub-graph of G_P and the nodes that are included in G_P but not G_{gt} to be empty. In training time, we extract the best matching subgraph of G_P to G_{gt} as G_S and compute the loss. In inference time, the prediction is the complete graph of the non-empty nodes. To extend our method to a non-complete graph, we may simply introduce a threshold to relation prediction, or other OOD methods including using the absolute distance in prototype classifier as discussed in B.3, or simply introduce a category for empty relation.

C Experiment details

We provide additional details about our experiments here, including the hyperparams search and hardware platforms, the details of the datasets, and the baselines.

C.1 Hyper-Params Search

Params	Distribution	Params	Distribution
lr	$\{1e-3, 2e-3, 5e-4\}$	th_S	$U(0.1, 0.5; 0.05)$ or None
K	$U(3, 9; 1)$	quota	$U(8, 32; 4)$
$\alpha_{overlap}$	$U(0.1, 0.25)$	d_{emb}	$\{64, 128, 256, 512\}$
$\alpha_{resources}$	$U(0.05, 0.2)$	$d_{sampler}$	$\{32, 64\}$
$\gamma_{cluster}$	$U(5e-3, 2e-2)$	d_{mapper}	$\{128, 256, 512\}$
σ	$\{2.5, 5, 10, 15, 25\}$		

We use Weights & Biases Sweep Biewald [2020] to do hyper-param search for our method. Table C.1 shows the distribution of our empirically significant parameters in our hyper-param search. $\alpha_{overlap}$ and $\alpha_{resources}$ are α_1 and α_2 in Formula 4. $U(a, b; s)$ means a discrete uniform distribution with a step size of s between a and b and $U(a, b)$ represents a uniform distribution between a and b . We use a combination of random search and grid search to explore the search space where the random search has been applied to discover the good traces, then using the visualization tool provided by Sweep, we get a smaller search space for a finer grid search. For different experiments, the final good range determined by the random search can be different, however, the distribution given by Table C.1 gives the common initial range that empirically likely covers the optimal sets to explore.

We run the experiments on our internal clusters. Two major workloads in our clusters have the following configuration: Quadro RTX 5000 \times 6 & Quadro RTX 8000 \times 1 GPUs + Intel(R) Xeon(R) Silver 4214R CPU @ 2.40GHz with 386 GB RAM and NVIDIA GeForce RTX 2080 Ti \times 7 GPUs + Intel(R) Xeon(R) Silver 4114 CPU with 192 GB RAM. We use PyTorch Lightning Falcon and The PyTorch Lightning team [2019] for running our experiments in parallel efficiently.

C.2 Details about datasets

Here, we give the basic statistics of the datasets we used, the split of train, test, and dev sets, and the details about how we create and preprocess the datasets.

C.2.1 LineWorld

We use the babyARC engine Wu et al. [2022] to synthesize the LineWorld dataset. All the objects in LineWorld are composed of lines as the basic concept with basic relations of parallel and perpendicular to each other. Each sample is an image covers 1 \sim 3 objects of “Lshape”, “Tshape”, “Eshape”, “Rectangle”, “Hshape”, “Cshape”, “Ashape”, and “Fshape”. Each shape may have a different size and color that is randomly selected from 3 available colors. The shapes

are non-overlapping and drawn in random positions on a pure white canvas. We synthesize 50000 samples in total and use an 8:1:1 split for train, dev, and test sets.

C.2.2 LineWorld-Grounding (LW-G)

We use the same babyARC engine to synthesize the LW-G dataset. The objects in LW-G are composed of lines as a basic concept with four relations to each other:

- Parallel:** the two lines are parallel.
- VerticalMid:** the two lines are vertical, with an endpoint of one line attached to the middle of another.
- VerticalEdge:** the two lines are vertical, with an endpoint of one line attached to an endpoint of another.
- VerticalSepa:** the two lines are vertical, but the endpoint of one line is not attached to another.

Each object is composed of a pattern. Apart from the 4 relationships as the basic pattern that simply samples two random lines following the 4 relations, we design 7 more complex patterns:

Patterns	Sampling process
F pattern	Sample line in a random position, sample the second line that “VerticalMid” to the first line, then sample a third line “VerticalEdge” to the first
E pattern	Sample one more line that “VerticalEdge” to the first line in a “Fpattern” with one endpoint attached to the unattached endpoint of the first line
A pattern	Sample one more line that is “Parallel” to the first line in a “Fpattern”, the line can be anywhere that does not overlap with the first line
C pattern	Sample one line in a random position, sample the second line that “VerticalEdge” to the first line, then sample a third line “VerticalEdge” to the first but attach to another endpoint
H pattern	Sample one line in a random position, sample the second line that “VerticalMid” to the first line, then sample a third line “Parallel” to the first
P pattern	Sample one more line that “VerticalEdge” to the second line in a “Fpattern” on the unattached endpoint
Rect	Sample one more line that “VerticalEdge” to the second line in a “Cpattern” on the unattached endpoint

Notice that the length and direction of sampled lines are random and the color of each line is randomly selected from two available colors, thus for example, a “F pattern” does not mean to give a “F” shape, i.e. the two parallel lines may have different direction and length, and it is the same for all other patterns.

Each sample is composed of an image of one object, a list of concepts (i.e. lines) where each concept consists of a mask that points out this concept in the image, and a list of relation tuples between the concepts (e.g. $(line1, line2, parallel)$). We generate 7000 samples in total, with a 5:1:1 split for train, dev, and test sets.

We evaluate the concepts in this way: suppose the model gives k candidates of the concepts, and k^2 relations between candidates, which is a complete graph G_C , we check whether G is included in G_C . We first assign c to the nearest candidates with minimal IoU, and we compute the mean IoU, then we compute the top-1 accuracy of the predicted relation based on the assignment of nodes.

For our model, the relation can be directly read from the 2-ary predicates, for baselines, we added a relation prediction head, that takes a pair of parts from the heatmap as input and then predicts a relation. The prediction head first uses a similar structure to our composition mapper, used to embed the outputted composition from each player for clustering, to embed the parts, then use a classifier to predict relation.

C.2.3 OmniGlot

The OmniGlot dataset is collected by Lake et al. [2015] who hired participants to draw 1623 different characters from 50 different alphabets online via Amazon’s Mechanical Turk Amazon [2005], each character has been drawn 20 times by different people. Each sample consisted of multiple stroke sequences of $[x, y, t]$ coordinates that recorded the strokes a participant used to draw the character.

We use the program given by Lake et al. [2015] to convert the stroke sequences to images. We use 24000, 1500, and 1500 images for train, test, and dev sets, and leave the remaining for the OG-G dataset.

C.2.4 OmniGlott-Grounding (OG-G)

OG-G is composed of the remaining 5811 samples, apart from the image of the character, each sample also contains a set of images of the strokes that are converted from the sequence of each stroke that composed the character as the ground truth. We use 4311, 750, and 750 samples for train, test, and dev sets.

C.2.5 ShapeNet5

ShapeNet5 consisted of all 20938 shapes of 5 categories (bed, chair, table, sofa, lamp), suggested by Achlioptas et al. [2019] that they are composed of shared basic elements, from ShapeNetCore v2 Chang et al. [2015], an updated version of the core ShapeNet dataset. There are many ways to represent 3D data including point clouds, meshes, voxels, Signed Distance Fields (SDF), and octrees. In order to make 3D shapes directly be applied to the same architecture with other datasets, we choose to voxelize the shapes, thus we can handle them by simply replacing 2D convolutions with 3D.

We use the binvox library Min [2004 - 2019], Nooruddin and Turk [2003] to voxelize the shapes into solid voxels (i.e., the interiors of shapes are filled). We apply 15938, 2500, and 2500 samples for train, test, and dev sets.

C.2.6 ShapeNet Transfer Learning

This transfer learning dataset consists of a pretraining set and finetuning sets. The pretraining set covers 11470 samples from 5 categories (chair, bench, cabinet, bookshelf, bathtub) that we regard as having similar basic compositions. Four finetuning sets correspond to four categories that share similar basic elements with the pretraining set: bed (233), lamp (532), sofa (550), and table (580), number of samples for each category is provided in brackets. We voxelize the samples the same way with ShapeNet5.

C.3 Baselines

Following Choudhury et al. [2021], we choose VGG19 pre-trained on ImageNet as the backbone for all three baselines in 2D data. For 3D data, we adopt MedicalNet Chen et al. [2019], a ResNet-based pre-trained model for 3D medical images (e.g. CT, MRI) which are high-resolution voxels, as the backbone.

DFC Collins et al. [2018] can be seen as doing spectral clustering over the features under certain conditions Ding et al. [2005]. Following Choudhury et al. [2021], we apply NMF to the activations of the last convolutional layer the backbone for both 2D and 3D data. DFC does not require training and applied NMF over the whole test set during inference in order to get the statistically consistent semantic parts across the test samples from the feature space.

UPD Choudhury et al. [2021] and **SCOPS** Hung et al. [2019] learn a part detector in self-supervised ways. We follow the methods from Choudhury et al. [2021] to implement UPD and SCOPS in our task. UPD and SCOPS require ground truth foregrounds for training, the ground truth foregrounds in our datasets are simply empty regions. We run hyperparam searches for both UPD and SCOPS to get their optimal results on our tasks.

D Additional experiments

In addition to our major experiment on unsupervised learning of transitional representation and transfer learning using transitional representation, we do extensive experiments to further excavate our proposed method, as well as evaluate the proposed metrics.

D.1 Ablation study

			LineWorld			OmniGlott		
			IoU	CIG	SP	MAE	CIG	SP
Base			91.3	26.3	28.4	2.5	31.8	23.8
~	+ Cluster		92.3	54.6	68.9	2.4	61.7	64.8
~	~	+ HOL	92.7	56.9	71.5	2.0	64.7	67.5
~	~	+ PPO	91.9	57.1	82.6	2.0	67.2	77.4
~	~	+ Attn.	94.9	56.2	70.8	1.8	63.4	66.8
~	~	+ LDM	91.7	53.6	66.9	3.2	59.9	62.8
Full model			94.3	58.0	82.6	1.8	68.5	77.6

We perform an ablation study on the proposed predicate clustering method, PPO tuning, as well as optimizations in LineWorld and OmniGlott datasets. The results are listed in Table D.1. “~” means repeat the above row.

“**Base**” means the model trained with only reconstruction loss and decomposition loss. Without dictionary learning, the model gives an arbitrary decomposition that reconstructs the input while meeting the game mechanisms, which generate compositions with diverse near-random shapes thus having low CIG and SP.

“**+ Cluster**” means adding clustering loss to the base model. With clustering loss, the model does the dictionary learning, which significantly improves the CIG and SP, since the model learns to find common elements to represent the data. It also shows that learning an efficient dictionary itself also results in simpler and more natural shapes. Although not sufficient to learn the human interpretable shapes.

“**+ HOL**” adds the higher-order predicate optimization to the model with clustering, it shows marginal improvement, which may be due to the low complexity of the shapes in our datasets, which do not contain too complex relationships that need to be depicted with higher-order predicates. And a better way of representing higher-order predicates may also lead to better results.

“**+ PPO**” adds a PPO tuning with heuristic reward to the model with clustering, it clearly improves the SP in both datasets due to the introduction of an explicit bias that guides the model to learn more natural shapes which shows the importance of feedback and environmental interactions.

“**+ Attn.**” adds attention layers to the model with clustering, it also gives marginal improvement which may be due to the relatively limited complexity of our dataset. Moreover, as discussed earlier, a better case for cross-attention is multimodal learning. And we do not test self-attention which we regard should be applied to larger datasets.

“**+ LDM**” uses a latent diffusion in the model with clustering, the result shows that using LDM has only limited harm on the model performance, compared to the efficiency improvement, the downside is quite acceptable.

In summary, the results show that dictionary learning plays a key role in learning transitional representation, while PPO can effectively improve the representation which shows the importance of environmental feedback; HOL and attention give marginal improvements in our datasets, however, in a more complex dataset and with better higher-order representation, they may give more improvements; LDM could improve model efficiency with little cost on performance which is necessary for scaling to larger inputs. Combining our qualitative study results shown in Figure 12, without feedback simulated by PPO, the learned transitional representation is on a *transition state* to a “symbol-like” representation.

D.2 Reinforcement Learning from Human Feedback

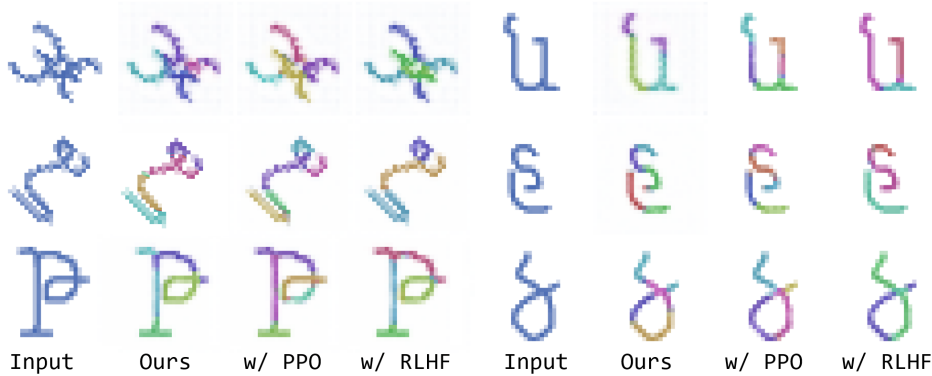


Figure 8: Examples of our methods, and our method using PPO with heuristic reward, and PPO with human feedback.

The key step from primitive symbols to real symbols in use in humans is through social interactions. We simulate the social feedback through the RL form Human Feedback (RLHF), we execute an experiment of tuning a training model with human feedback by displaying the current decomposition (visual parts) to the human trainer in Weights & Biases Biewald [2020], then human input their rating in the training terminal. Figure 8 shows examples of our methods before and after PPO, and RLHF, we can see that compared to the shape of compositions found by the model before PPO, the after PPO model tends to use more continuous and solid shapes, which may result in avoiding shapes like circles, RLHF model are more “brave” that can learn the shapes that not encouraged by the heuristic reward but looks more interpretable to human.

We also evaluate the model with only PPO and with RLHF. The results in Table D.2 shows that the improvement of interpretability is not clearly reflected in the metrics with little improvement. It shows a limitation of the metrics in that the interpretability improvement cannot be fully reflected in the metrics. This is also a main challenge in many

	LineWorld			OmniGlott		
	IoU	CIG	SP	MAE	CIG	SP
w/o RLHF	94.3	58.0	82.6	1.8	68.5	77.6
w/ RLHF	94.1	58.9	83.1	1.8	68.7	78.2

content generative disciplines that lack a low-cost way to evaluate the generation quality, for example, BLEU Papineni et al. [2002] in machine translation has been criticized for a long time for not effectively evaluating the quality of generated sentences.

This also shows that the “*last mile problem*”, which means getting the ideal human interpretable representation from a good feasible one, is hard, and one important reason is that it is hard to distinguish the ideal one from other good ones. A real embodied learning Gupta et al. [2021] in the environment with phylogenetic interactions may be the key to this problem as discussed.

D.3 Latent space visualization

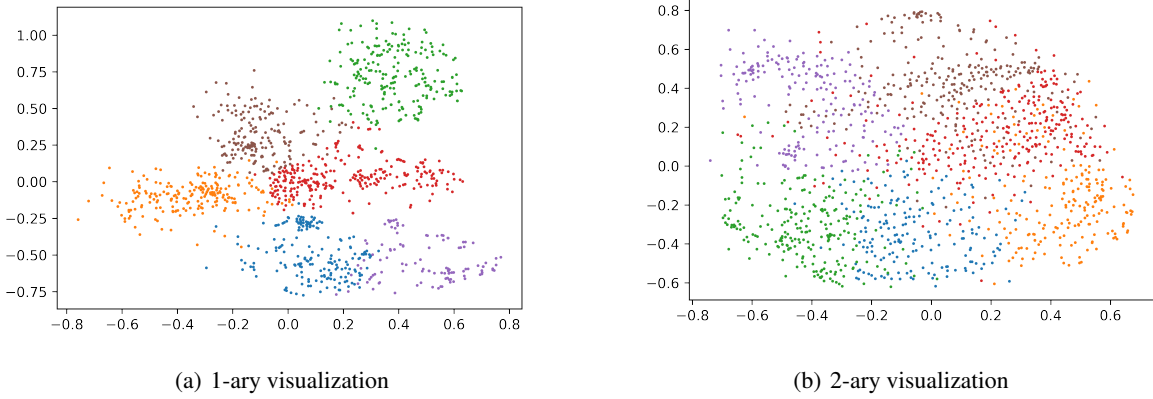


Figure 9: t-SNE for the latent space of 1 and 2-ary terms in the decompositions of samples in the LineWorld test set.

In dictionary learning, we expect the model to learn to explain data with common basic elements, thus the terms that belong to the same dictionary item should be similar to each other. We visualize the latent space of the compositions associated with 1-ary and 2-ary predicates decomposed by our method in the LineWorld test set.

For each input x , we obtain N visual parts from N players, and the parts can compose N^2 pairs, as we discussed earlier, we filter out the unwanted parts and pairs, then embed them into 1 and 2-ary representations \vec{m}_1 and \vec{m}_2 , and we assign each term to the nearest prototype, which provides labels \vec{y}_1 and \vec{y}_2 that designate the id of the prototype assigned to each term. Then we mark the representations and labels for all samples in the test set X as \vec{M}_1, \vec{M}_2 and \vec{Y}_1, \vec{Y}_2 .

We run tSNE on \vec{M}_1 and \vec{M}_2 respectively then assign each point different color according to their label \vec{Y}_1 and \vec{Y}_2 , the result is shown in Figure 9. We can see that the model learns a well-separable latent space for 1-ary predicates, which means that the parts that correspond to the same prototype are similar to each other. For 2-ary predicates, the space is still clustered which means the pairs shown in the decompositions by the model can be categorized into few patterns, although it does not as concentrated and clearly separable as in 1-ary, we hypothesize that it is caused by our pair sampling strategy that removes empty pairs and then randomly samples which may cover many redundant samples, and our pair representation is naive that simply adding two parts.

It shows that better sampling methods that discover potentially related pairs can be helpful, it is similar to a key challenge in contrastive learning Jaiswal et al. [2020] learning is how to sample positive and negative samples when we regard pairs with relations are positive samples. The sampling method could make a large difference, without an efficient sampling strategy, the sample efficiency in InstDisc Wu et al. [2018] is largely lower than later methods.

D.4 Analysis of CIG

To compute the CIG of a model, we first use the model to decompose every sample x in the test set to parts \vec{x} , and get the set \vec{X} of all the parts decomposed from the test set. Then we build another set of parts \vec{X}_{rand} by randomly sampling parts from samples in the test set. We implement a sampling by generating a mask on the input with normal distribution on each position. With the two part sets, when then compute their MCE to get MCE_{model} and MCE_{rand} thus we can compute the CIG. We first reduce the dimension of parts, then run a K-Means clustering.

The dimension reduction method may influence fairness, we considered three typical image dimension reduction techniques, PCA, Auto-Encoder (AE), and a pre-trained CNN, VGG19. The comparison of the three methods is provided in Table D.4. “Reference” in LineWorld is computed over a set of common elements including lines and two vertical lines on mid or edge (i.e. “L” and “T” shapes) with different lengths, colors, positions, and directions; in OmniGlott, the “Reference” is the set of the ground-truth strokes. Since AE needs training, different runs may give different results, we train AE ten times in each dataset and give the average results and test the variance, it shows that the AE-based CIG is stable with about 2.85% variance in different runs.

	LineWorld			OmniGlott		
	AE	VGG19	PCA	AE	VGG19	PCA
Reference	64.6 ($\pm 3.57\%$)	57.1	16.0	75.8 ($\pm 2.49\%$)	67.2	28.5
DFF Collins et al. [2018]	33.1 ($\pm 2.23\%$)	29.3	8.6	36.9 ($\pm 3.08\%$)	32.2	11.8
SCOPS Hung et al. [2019]	35.6 ($\pm 3.01\%$)	32.3	8.8	38.6 ($\pm 2.63\%$)	35.4	12.0
UPD Choudhury et al. [2021]	36.3 ($\pm 2.94\%$)	32.7	9.4	42.8 ($\pm 2.45\%$)	37.8	13.2
Ours	58.0 ($\pm 2.79\%$)	51.5	13.0	68.5 ($\pm 3.32\%$)	60.6	20.3

We applied AE as the default dimension reduction method in our experiments, since PCA work is unsatisfied, while the pre-trained VGG can only work for image data and AE gives a similar result to VGG, we expect a method that can provide a fair differentiation while being able to generalize to all kinds of data.

We train a *common* AE when comparing different methods, for each dataset, we train an AE on that dataset and then use this AE to compute and compare the CIG of different methods trained on this dataset We run K-Means with a fixed K, for OmniGlott and ShapeNet5, we set K as 32, and for LineWorld, we choose 10, which is the number of parts we regard adequate for composing the dataset.

D.5 Analysis of Shape Score

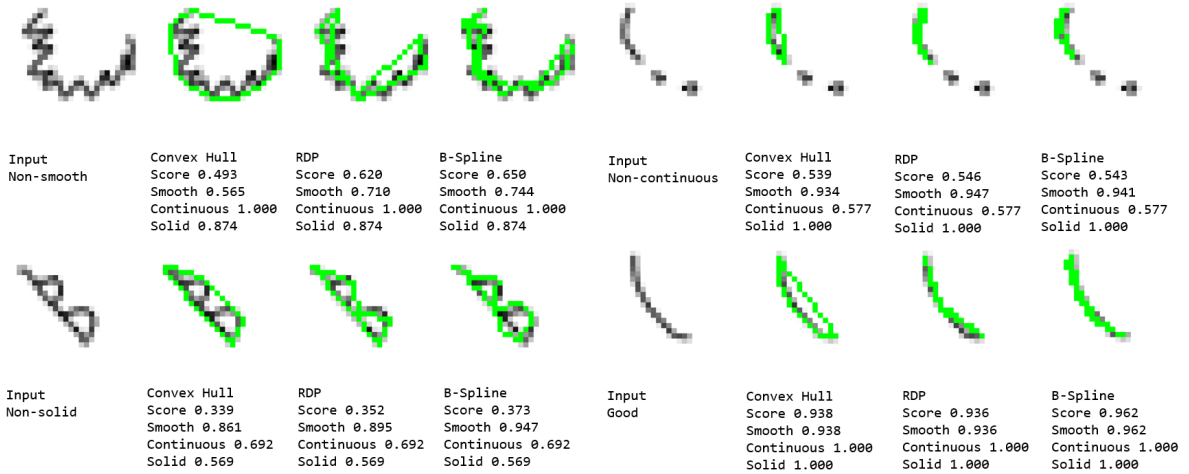


Figure 10: Visualization of the shape score under different cases and different smooth method, the green lines are the smoothed shape.

We design a heuristic shape score to simulate environmental feedback that emulates whether such a shape will happen in natural real work. It evaluates from 3 aspects:

- Solid: no empty parts inside the shape, strokes, and objects in the real world are solid
- Smooth: the surfaces or contours are smooth, which is common in natural shapes
- Continuous: the shape is a continuous whole instead of segmented parts

For 2D data we use *findContours* in OpenCV to give the contours of segments inside a composition, we evaluate the continuity by the ratio R_{cont} between the area of the largest contours and the sum of areas of all contours. And then we evaluate the smoothness and solidity of the largest segment, for solidity, we compute the ratio R_{solid} between the area circled by the contour and the area of the segment, if there are holes inside, then R_{solid} will be less than 1, for smoothness, we compute the ratio R_{smooth} between the perimeter of a smoothed contour and an original one. The shape score is computed as $R_{cont} \times R_{solid} \times R_{smooth}$, which is normalized between 0 and 1.

We compare three ways to smooth the contour, minimal convex hull, Ramer–Douglas–Peucker (RDP) algorithm, and B-spline interpolation in LineWorld and OmniGlut dataset, the result is listed in Table D.5, where the three methods are marked as “Hull”, “RDP” and “Spline” respectively, “Reference” is the same with Table D.4. And “Random” is obtained with the random sampling method in computing CIG.

	LineWorld			OmniGlut		
	Hull	RDP	Spline	Hull	RDP	Spline
Reference	89.7	99.5	97.9	80.0	86.1	82.9
Random	19.1	14.2	17.4	13.1	14.2	16.3
DFE Collins et al. [2018]	35.8	38.3	40.5	29.4	33.3	31.2
SCOPS Hung et al. [2019]	42.3	42.4	47.7	33.1	38.9	35.4
UPD Choudhury et al. [2021]	41.9	42.8	46.1	32.8	37.4	35.0
Ours	79.6	82.6	86.8	70.5	77.6	76.6

In our experiments, we apply RDP as the default smooth method, since the convex hull is too strict that prefers straight or round shapes, B-Spline and RDP gives similar results but RDP gives slightly better differentiation. We further visualize the scores under different cases and different smooth methods in Figure 10, we can see that RDP gives a smoother shape that fits the original shape better.

For 3D data we convert voxel into point cloud, then use DBSCAN clustering to get segments, then compute R_{cont} and evaluate the largest segment similar to 2D, for solidity, we compute ratio R_{solid} between an encircled volume which is obtained by the Alpha Shape algorithm and the volume occupied by the segment, for smoothness, we compute ratio R_{smooth} between the surface area of the minimal convex hull of the shape and the surface area of the alpha shape.

As a generalization of the convex hull, the alpha shape can be regarded as a smoothed version of the shape, and the minimal convex hull is the extreme case with maximal smoothness. The score is computed in the same way with 2D as $R_{cont} \times R_{solid} \times R_{smooth}$, and also normalized between 0 and 1.

We also use this shape score as the reward function in our PPO tuning. Although not able to cover all kinds of natural shapes, for example, the solidity may discourage the circles, the shape score still gives a good feasible set that provides much more human interpretable results by avoiding the apparently unnatural ones that we assume a shape cannot be segmented otherwise its multiple shapes, most natural shapes do not have holes inside, and natural shapes are smooth. Such a heuristic can be attributed to the *principle of least effort* as such shape will be easier to draw or produce, for example, Johnson et al. [2008] shows that painters tend to produce smoother strokes. Our experiment results especially the human qualitative studies that will be discussed later shows that the shape score gives a good prediction for interpretability, we can expect that a better simulation of the real environment can give better performance.

D.6 Human Qualitative Studies on OmniGlot

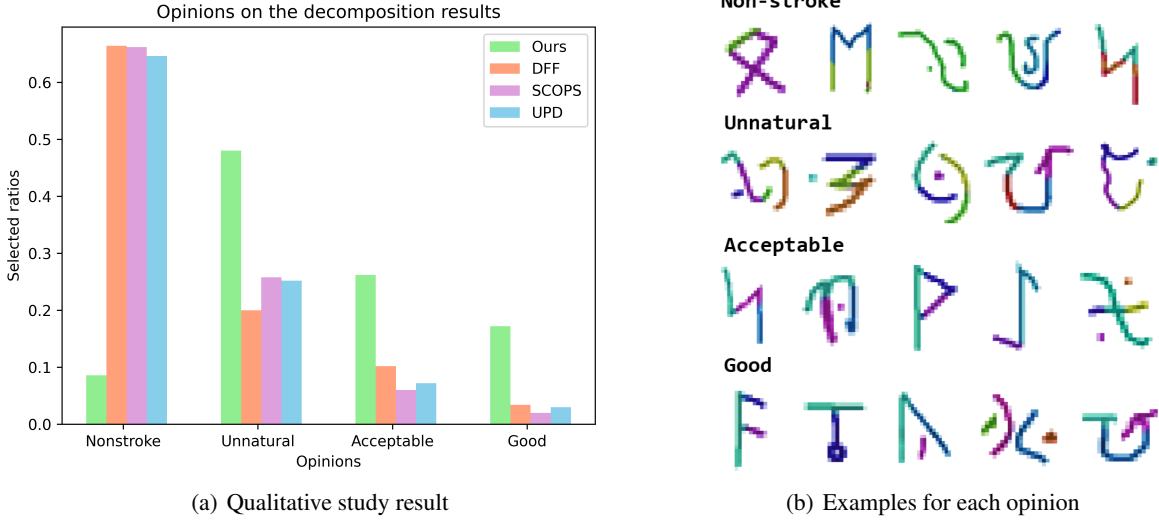


Figure 11: Results of the qualitative study and examples of results annotated with each option.

To evaluate the human interoperability of the learned representation that does not directly give by the metric, we design a qualitative study on our method and the baselines on the results of the OmniGlot test set. We randomly choose 500 samples from the OmniGlot test set separately for each method then let these methods decompose the samples which in total gives 2000 decomposed results.

We use Google Vertex AI Google [2021] data labeling service to evaluate those results by Google annotators. For each sample, we hire 3 annotators to label and average the results to improve accuracy. We publish an image annotation task that given a decomposed sample, the annotator needs to give one of four opinions which are explained in an instruction that is required to be read before an annotation task start. The 2000 samples are mixed up to avoid the annotator getting aware of which method produced the result which can be a confounder that influences their judgment, and the samples are randomly assigned to the annotators.

This results in a small data set on the human rating towards machine decomposition of hand-written strokes. We make this data set publicly available and the annotation instruction is provided with the dataset. Figure 11(b) provides examples in this data set that are annotated as the four options, interpretation for those opinions can be found in the instruction.

Figure 11(a) shows the result, we can see that around 65% of results from the baselines are not regarded as effective strokes, and only around 10% are rated as acceptable or good, and from our investigation, many of the good samples from baselines are simple characters with only one or two strokes. On the contrary, less than 10% of samples from our method are marked as “Non-stroke”, and nearly half of the samples are recognized as acceptable and good. Major complaints are still unnatural, which shows a clear distinction compared to the baselines who are struggling in giving effective strokes, and our method can

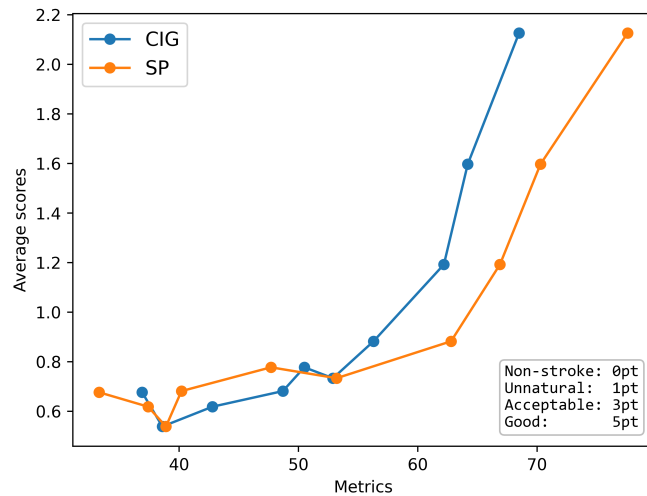


Figure 12: The emergence of interpretability compared to metrics. It shows a transition to “symbol-like” representation.

effectively learn a dictionary of human interpretable compositions.

We further do a study on the emergence of interpretability compared to our proposed metrics, we additionally train 6 models with SP and CIG nearly evenly distributed between ours and the baselines through the early stop. And then do the human evaluation in the same way above for each model to get ratings of 10 models in total. We define a “Non-stroke” as 0 points, “Unnatural” as 1 point, “Acceptable” as 3 points, and “Good” as 5 points, then compute the average scores getting by each model to draw a figure of metrics versus the scores. A higher score means a higher interpretability rated by human annotators.

The results are shown in Figure 12. It shows that there is an emergence of interpretability compared to the metrics, the SP and CIG are not linearly related to the interpretability, however, still overall positively correlated which means that both of them give a good prediction of interpretability, and indicate that high SP and CIG might be *necessary but not sufficient conditions* for good interpretability.

D.7 Decentralized training

An advantage of a Game-Theory-based formulation is that it enables the model to work in a decentralized way, which may largely improve the scalability as shown in EigenGame Gemp et al. [2021]. In our method, players communicate with each other by broadcasting their new move after each time step. In a centralized environment, the communication is local, and the broadcast can always successfully deliver while in a decentralized case, there is a risk of out-of-sync. This means that there is a probability p that a player fails to broadcast their latest move, thus other players do not get an update and assume the player does not move in this round.

We do an experiment by simulating this environment to the robustness of our method under the out-of-sync risk p . The results are available in Table D.7, they show that our model has limited robustness to the out-of-sync risk, when $p = 0.05$, the average performance drop for each metric except MAE in OmniGlott is 3.13%, when $p = 0.10$, the drop comes to 9.34%, which is not very ideal but still around the border of the emergence of interpretability according to Figure 12 thus we set it as the threshold for acceptable performance drop, and the performance drop in $p = 0.20$ is serious and cannot learn effective transitional representation, and for $p = 0.30$ the model cannot converge. As a result, the model has limited robustness when out-of-sync probability $p \leq 0.10$.

	LineWorld			OmniGlott		
	IoU	CIG	SP	MAE	CIG	SP
$p=0.05$	89.7	56.0	79.7	2.2	66.5	76.9
$p=0.10$	85.7	52.8	74.6	3.4	61.8	70.5
$p=0.20$	67.4	39.8	43.2	8.6	42.3	44.7
$p=0.30$	Diverge			Diverge		

There are more potential designs for decentralized learning apart from one model one player way, a possible design is to allow each model to handle multiple players and learn its own dictionary with additional game mechanisms as a way of ensembling or bagging Ramesh and Chaudhari [2022], and the multiple dictionaries learning in TDL is distributed to multiple independent models.

E Limitation

In this work, we introduce a novel problem, symbol emergence and transitional representation, to machine learning that may become the key to learning System II intelligence. And a simple, flexible, and effective TDL framework to solve this problem along with evaluation metrics CIG and SP, and implemented by the modular model architecture.

As an experimental method for a novel problem, our work still has limitations, firstly, we only evaluated in a basic case of transitional representation where the logic variables are the visual parts, while in the human mind, we use auxiliary variables and multimodal multisource information to think. And the given interpretations are simply evaluated in the pixel space in the form of segmentation, while humans care more about consistency in meaning and using diverse logical structures. The objects in tasks are also relatively simple although they are abstract while real-world objects after abstraction can also look simple which is shown in our experiment in the voxelized ShapeNet.

Secondly, our work only shows the emergence of the transitional representation which is an important problem and the basis for solving the problem of symbolic thinking from essence, however, this work has not touched the most desirable part, symbolic reasoning.

Thirdly, the model still trains by sampling full sequences, which is feasible for our needs, but it is not efficient and is a key detriment to its scalability, although it is also restricted by current research in multi-source diffusion. There are also other optimizations that can be made in our implementation like a more efficient clustering method.

Overall, those limitations largely come from the fact that we are facing a novel, broad, and challenging problem with novel designs, thus we choose to evaluate on relatively simple but typical case of visual compositionality, focus on the core problem of transitional representation, and using a conservative implementation of the full sequence sampling.

F Broader Impact

We show how symbolic knowledge may emerge from neural networks in this work by learning concepts and relations in a grid world of lines and finding strokes in characters and parts in shapes. As an important cognitive science problem, our work may inspire researchers to further understand how symbols emerged in natural and artificial cognitive systems from a more fundamental view, and further help us to understand how symbolic thinking emerged.

The transitional representation between neural representation and symbolic knowledge may potentially support the emergence of a model that embeds System II intelligence and better interpretability through self-supervised learning, as symbols are the basis for symbolic thinking and also having better interpretability, and also benefits the Neural-Symbolic models that try to reconcile the neural and symbolic modules since a transitional representation provides the required information for both. Furthermore, the metrics and evaluation methods we introduced can also assist future researchers in this discipline in developing new methods for solving these challenging problems.

We see no negative impact of this work. Our method is still in its early stage which shows simple symbol emergence abilities with an extensible framework. We see that the model with better symbol emergence ability and further symbolic thinking can lead to more logical, interpretable, causal, and controllable intelligence. This can help us build safer, smarter, and easier-to-use AI for everyone.

G Quantitative samples and comparison on OmniGlott

We randomly sample 260 characters from the OmniGlott test set for each of Ours and baseline models for additional comparison and qualitative study. Compared to baselines, with a dictionary learning paradigm, our model can learn the concepts like lines, and curves to represent the data, which are close to the human strokes. Different parts are colored differently for each sample, color may mix due to a pixel may belong to different parts with different confidence, lower color mix indicates higher confidence.

G.1 Ours

